ASCE

Quantifying the Impact of the Inherent Coupling of Particle-Scale Variability on Granular Soil Behavior: A Micromechanical Study

Deyun Liu, Ph.D.[1]; Meng-Ze Lyu, Ph.D., M.ASCE[2]; and Jidong Zhao, Ph.D., M.ASCE[3]

Abstract: This study investigates how the inherent discreteness and coupled variability of particle-scale properties, specifically interparticle friction (μ_s) and shear modulus (G_p), affect macroscale soil behavior. To achieve a comprehensive probabilistic quantification, copula theory was employed to model the joint dependence between these particle properties, capturing the inherent property uncertainty in granular materials. The results reveal that coupled particle property uncertainties significantly influence macroscale parameters, including the stress ratio, void ratio, and small-strain stiffness, which are strongly associated with desired packing densities and soil states. Notably, the uncertainties of mechanical behaviors converge at the critical state, regardless of packing density, consistent with conventional soil mechanics. In contrast, the impact of coupled μ_s and G_p on particle-scale stress transmission was negligible, with particle size distribution emerging as the dominant factor. Furthermore, a decoupled multiprobability density evolution method (M-PDEM) was introduced to investigate nonlinear dependencies among macroscale parameters. This approach unveiled observable probabilistic interconnections among stress ratio, void ratio, and coordination number. Such interdependencies, often overlooked in conventional deterministic models, highlight the importance of uncertainty quantification for accurate soil behavior prediction. By integrating copula theory with the decoupled M-PDEM framework, the study offers a robust method for tracing the propagation of microscale uncertainties to macroscale responses, bridging the gap between particle-level variability and engineering-scale behavior. These insights can inform probabilistic geotechnical design methodologies, improve the reliability of numerical simulations, and enhance our understanding of soil behavior under realistic loading and material variability conditions. This study establishes a framework to capture the inherent discreteness and coupling of particle-scale properties, revealing micromechanical mechanisms that govern macroscale soil behavior and strengthening the physical basis for geotechnical analysis and design.
DOI: 10.1061/JGGEFK.GTENG-14000.

Author keywords: Stochastic discrete-element method; Uncertainty quantification; Granular material; Soil behavior; Probabilistic dependence; Decoupled multiprobability density evolution method (M-PDEM).

Introduction

Capturing the microscale interactions and structural evolution among particles is essential for understanding the macroscale mechanical behavior of granular soils. However, it remains experimentally challenging to directly observe and quantify particle-scale interactions within granular assemblies (e.g., Snoeijer et al. 2004; Majmudar and Behringer 2005). Among available modeling techniques, the discrete-element method (DEM) enables direct simulation of particle-scale interactions, offering micromechanical insights that enhance understanding of macroscopic soil behavior relevant to engineering applications (e.g., Cundall and Strack 1979; O'Sullivan 2011). Beyond its role in fundamental studies, DEM-based representative volume elements (RVEs) are increasingly used in multiscale geomechanical frameworks, either to inform constitutive model development or to bridge microscale behavior with engineering-scale performance through coupled methods such as DEM–FEM (e.g., Guo and Zhao 2014) and DEM–MPM (Chen et al. 2023).

Owing to their discrete nature and complex geological origins, granular soils may exhibit potential variation in their particle shape, size, and mechanical properties. These efforts aim to achieve a more authentic representation of granular materials by accurately modeling key physical properties. For instance, increasing studies have focused on simulating realistic particle shapes and sizes, using techniques such as CT scanning to obtain various particle morphology (e.g., Wu et al. 2022; Zhao et al. 2023). Other studies have emphasized realistic particle size distributions (PSDs), including those of gap-graded soils, to better replicate material behavior (e.g., Shire et al. 2014; Sufian et al. 2021; Liu et al. 2023). Additionally, contact models have evolved from simpler linear approaches to more sophisticated models, such as the Hertz–Mindlin model, which, based on experimental evidence, more accurately represents the complex interactions between particles (e.g., Kuhn and Daouadji 2018; Zhao et al. 2018). Despite the increasing significance of multiscale analysis, which necessitates accurate particle-scale representations, fewer studies have addressed the discrete nature and variability of particle-scale properties. While some studies have explored the sensitivity of simulations to individual parameters, such as interparticle friction (μ_s) (e.g., Huang et al. 2014) and shear modulus (G_p)

[1]Associate Professor, Dept. of Geotechnical Engineering, Tongji Univ., Shanghai 200092, China; Dept. of Civil and Environmental Engineering, Hong Kong Univ. of Science and Technology, Hong Kong 999077, China. Email: 25044@tongji.edu.cn; deyunliu@ust.hk

[2]Research Fellow, Institute for Risk and Reliability, Leibniz Univ. Hannover, Hannover 30167, Germany (corresponding author). ORCID: https://orcid.org/0000-0002-8932-2617. Email: lyumz@ust.hk

[3]Professor, Dept. of Civil and Environmental Engineering, Hong Kong Univ. of Science and Technology, Hong Kong 999077, China. Email: jzhao@ust.hk

Note. This manuscript was submitted on February 20, 2025; approved on August 1, 2025; published online on November 17, 2025. Discussion period open until April 17, 2026; separate discussions must be submitted for individual papers. This paper is part of the ***Journal of Geotechnical and Geoenvironmental Engineering***, © ASCE, ISSN 1090-0241.

(e.g., Yan et al. 2015), many still rely on global average values for micromechanical parameters. For instance, in quartz sand, DEM models using the Hertz–Mindlin contact law typically assign fixed average values for interparticle friction (μ_s of 0.25), shear modulus (G_p of 29.17 GPa), and Poisson's ratio (υ of 0.2) (e.g., Barreto 2008; Huang 2014; Liu et al. 2021).

This approach overlooks the inherent variability in particle properties, limiting simulation accuracy (Zhou et al. 2016; Tao et al. 2020). It neglects the intrinsic variability of granular materials and the coupling effects between particle-scale parameters, reducing simulation realism and hindering accurate representation of particle properties. This gap arises from the lack of systematic experimental quantification of micromechanical parameters across particles. Recent advancements by Senetakis and Coop (2014) and Nardelli and Coop (2019) have introduced custom interparticle loading apparatuses, providing crucial data to quantify particle-scale parameters and enabling more realistic simulations of particle properties.

However, the large number of particles in granular materials means that experimental data typically represent only a limited subset of the system. Consequently, using deterministic or mean values to model the overall behavior may inadequately reflect the underlying heterogeneity of the system. Besides, significant uncertainty in particle properties has been increasingly recognized (e.g., Cardoso et al. 2016; He et al. 2019; Nardelli and Coop 2019; Tian and Senetakis 2022). These uncertainties stem from measurement limitations, human observation errors, and inherent natural variability due to geological processes such as sediment deposition, weathering, and biological activity (e.g., Baveye et al. 1998). These both motivate the adoption of probabilistic modeling frameworks capable of systematically accounting for data sparsity and capturing the stochastic nature of particle-scale variability in a physically meaningful manner.

Besides, uncertainty is a critical factor in engineering design, influencing practical outcomes (e.g., Phoon and Kulhawy 2008; Jiang et al. 2014). In natural materials, uncertainty stems from geological history and physical conditions, causing variability in material properties (Lumb 1966; Vanmarcke 1977; Phoon and Kulhawy 1999). For engineered materials, it arises from production processes, heterogeneity, and manufacturing parameters, affecting concrete (Bazant and Planas 2019), composites (Daniel 1994), and metals (DebRoy et al. 2018). Ignoring uncertainty in geotechnical applications can lead to inaccurate predictions and failures, such as compromised bearing capacity (Griffiths and Fenton 2001), settlement (Phoon and Kulhawy 1999), slope failures (Dyson and Tolooiyan 2019), and inaccuracies in pile load capacity (Baecher and Christian 2005).

Advances in computational methods have integrated uncertainty into engineering analysis. The finite-element method (FEM), combined with Monte Carlo simulations (MCS), enhances reliability and risk assessment in applications such as slope stability (Mahadevan and Haldar 1991; Potts et al. 2001; Griffiths and Fenton 2004; Griffiths et al. 2009) and structural engineering (e.g., Xu and Zhai 2017; Afshari and Pourtakdoust 2018; Ang et al. 2021). In geotechnical engineering, studies highlight the impact of soil parameter uncertainty—particularly shear strength, friction angle, and hydraulic properties—on failure probability and performance (Jiang et al. 2014). These findings underscore the limitations of deterministic models in capturing system complexities.

Previous studies have mainly focused on quantifying macroscale uncertainties in soil behavior and their impact on engineering performance. These uncertainties, often evaluated through tests such as the standard penetration test, exhibit significant spatial variability (Basarir et al. 2010; Rahimi et al. 2020). In computational frameworks such as the FEM, constitutive models describe stress–strain relationships, with uncertainty introduced by variations in soil parameters. However, the FEM assumes material continuity and homogeneity, which may oversimplify the complexities of granular soils.

Nevertheless, capturing realistic particle-scale properties with uncertainty has been relatively rare, due to the historical lack of experimental techniques for measuring micromechanical properties across particles and the absence of theoretical frameworks capable of managing the high computational costs associated with uncertainty propagation from the microscale to the macroscale. While MCS are commonly used for their simplicity and accuracy (e.g., James 1980; Elishakoff 2003), they often require $\sim 10^4$ simulations to ensure reliability (Li and Wang 2023), making them prohibitively expensive for DEM-based analyses. Alternative moment methods—such as high-order moments (Zhao and Lu 2007; Low 2013), fractional moments (Xu and Kong 2018), and linear moments (Zhang et al. 2021)—are more efficient but struggle to fully capture nonlinear probabilistic behavior. The probability density evolution method (PDEM) (Li and Chen 2009) offers a promising solution, generating a probability density function (PDF) surface with only $\sim 10^2$ simulations (Chen et al. 2020, 2024), significantly reducing computational costs and enabling the study of granular assemblies while accounting for the discrete nature of particle-scale parameters. The development of these tools has enabled recent studies (e.g., Liu and Lyu 2023a, 2025) to incorporate particle property uncertainties and assess their propagation from particle-scale to macroscale soil behavior. By analyzing PDFs and cumulative distribution functions (CDFs), these studies have demonstrated the significant influence of μ_s and G_p on the stress ratio, void ratio, and small-strain stiffness (G_0) across axial strains, providing a more comprehensive understanding of granular soil behavior.

However, existing studies have primarily examined marginal PDFs or individual parameter uncertainties, overlooking the coupling effects between particle-scale parameters such as μ_s, G_p, υ. Specifically, a coupling relationship between μ_s and G_p has been observed, where higher μ_s corresponds to lower G_p and vice versa, reflecting the inherent trend of these parameters (e.g., Sandeep et al. 2018; Liu et al. 2024a). This gap arises due to the lack of an appreciative framework to account for the coupling effects of particle-scale parameters. Therefore, a comprehensive methodological framework is needed to capture coupled uncertainties, enabling a more robust multiscale uncertainty analysis. Recent advancements, the decoupled multi-PDEM (M-PDEM) framework (Lyu et al. 2024e), provide the first opportunity to analyze joint probability distributions of interdependent macroscale responses, moving toward more realistic modeling of granular materials.

This study therefore presents an enhanced framework that captures the coupling relationships between particle-scale parameters, such as μ_s and G_p, which accounts for the natural variability of particle properties. This approach aims to model granular materials more realistically and provides a comprehensive understanding of macroscale soil behavior, offering valuable insights for engineering design and decision-making. Additionally, it contributes to solving multiscale engineering problems, where understanding particle-scale heterogeneity is crucial for reliable design and analysis.

Methodology

This study develops a framework to model granular materials more realistically by capturing the coupled variability of particle-scale

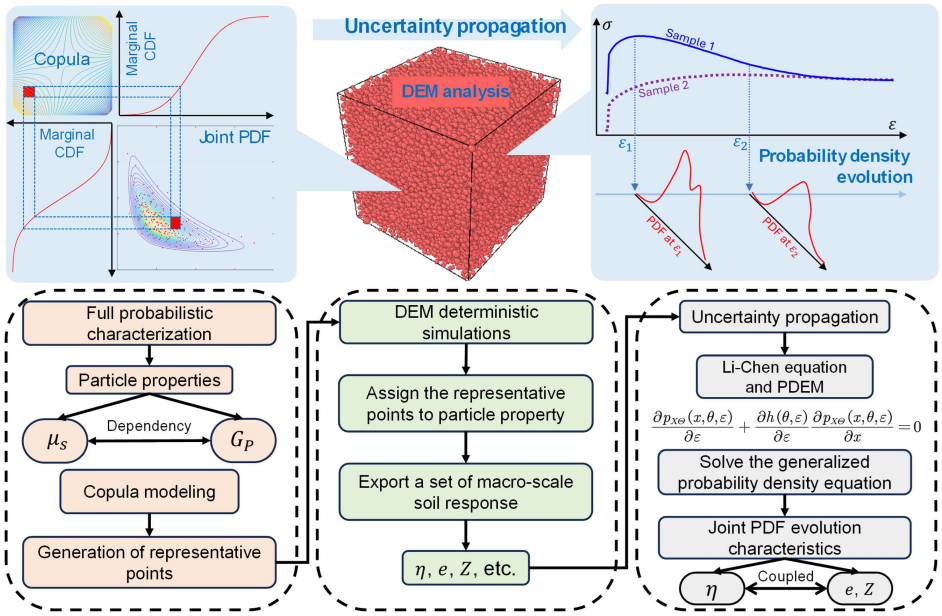

Fig. 1. Numerical procedure of this study.

properties and their influence on macroscale soil behavior. The methodology includes three key steps (Fig. 1):

1. Coupled variability characterization: Copula theory is used to quantify the dependency between μ_s and G_p, reflecting inherent correlations observed in real granular materials beyond conventional independent or average parameter assumptions.
2. Computational mechanical analysis: DEM is applied to simulate how realistic particle-scale variability affects macroscale behavior, leveraging its strength in representing discrete particle interactions at the RVE scale.
3. Uncertainty propagation: To propagate particle-scale variability to macroscale responses without prohibitive computational cost, an efficient probabilistic method of PDEM is adopted as an alternative to conventional Monte Carlo simulations. Each of these steps will be discussed in detail.

Probabilistic Dependence Quantification of Particle Properties

Although direct quantification of particle-scale properties has been relatively rare in prior research, some studies have sought to address this gap and quantify key particle properties, including μ_s and G_p (e.g., Senetakis and Coop 2014; Nardelli and Coop 2019). These investigations revealed significant uncertainties in particle properties and identified strong probabilistic dependencies among these particle-scale properties, as shown in Fig. 2(a). In this study, μ_s and G_p were chosen as the primary properties due to their pivotal roles in the Hertz–Mindlin contact model and their relative accessibility for experimental measurement. Although quantifying a wider range of particle-scale properties remains challenging, the relative precision with which these two parameters can be measured makes them well-suited for analyzing coupled particle-scale uncertainties and their effects on macroscale soil behavior.

The experimental values of μ_s and G_p were sourced from an extensive literature database on natural quartz sands (Nardelli et al. 2017; Senetakis and Sandeep 2017; Sandeep et al. 2018; Liu et al. 2019; Nardelli and Coop 2019). While μ_s was directly obtained, G_p was estimated from the particle Young's modulus (E_p) using the relation $G_p = E_p/[2(1+\upsilon)]$, where a Poisson's ratio (υ) of 0.2 was assumed. It is important to note that this assumption may introduce inaccuracies, as direct measurement of υ remains technically challenging. The E_p values were derived using Hertzian contact theory (Hertz 1882), by fitting normal compression curves, following the methodologies outlined by Nardelli et al. (2017) and Sandeep and Senetakis (2018). The derived E_p values may be subject to uncertainty due to the limitations of the Hertz model in accounting for particle roughness. In stochastic engineering, it is crucial to address both aleatory uncertainty (e.g., mineralogical variations) and epistemic uncertainty (e.g., model constraints) concurrently.

Linear correlation is inadequate for capturing the complex and inherently nonlinear dependencies observed in granular material behavior. Instead, a copula-based framework offers greater flexibility and precision in modeling uncertainties and has been widely utilized in reliability and risk studies across various engineering disciplines (e.g., Tao et al. 2020; Song et al. 2021; Chen and Lyu 2022; Luo and Ai 2022; Hai and Lyu 2023; Lyu et al. 2024b, c, d). Copulas enable the decomposition of multivariate distributions into their one-dimensional marginal distributions and a copula function that captures the dependencies among variables. This approach is particularly advantageous as it enables the realistic modeling of inherent dependencies between particle-scale properties, ensuring that the coupled variability observed in real granular materials is faithfully represented.

This section outlines the theoretical foundation of copula theory and details the numerical implementation process for configuring probabilistic dependencies using a copula-based framework. For illustrative purposes, the joint PDF of two correlated variables, such as the particle properties μ_s and G_p (denoted as Θ_1 and Θ_2), can be expressed as (Nelsen 2006)

$$p_{\boldsymbol{\Theta}}(\theta_1,\theta_2) = c_{\boldsymbol{\Theta}}[F_{\Theta_1}(\theta_1), F_{\Theta_2}(\theta_2)]\, p_{\Theta_1}(\theta_1)\, p_{\Theta_2}(\theta_2) \qquad (1)$$

where $c_{\boldsymbol{\Theta}}(\cdot,\cdot)$ = copula density function describing the dependency between soil properties μ_s and G_p; $p_{\Theta_1}(\theta_1)$ and $p_{\Theta_2}(\theta_2)$ = marginal PDFs of μ_s and G_p, respectively; and $F_{\Theta_1}(\theta_1)$ and $F_{\Theta_2}(\theta_2)$ = corresponding CDFs. If n pairs of observed samples of μ_s and

J. Geotech. Geoenviron. Eng., 2026, 152(2): 04025181

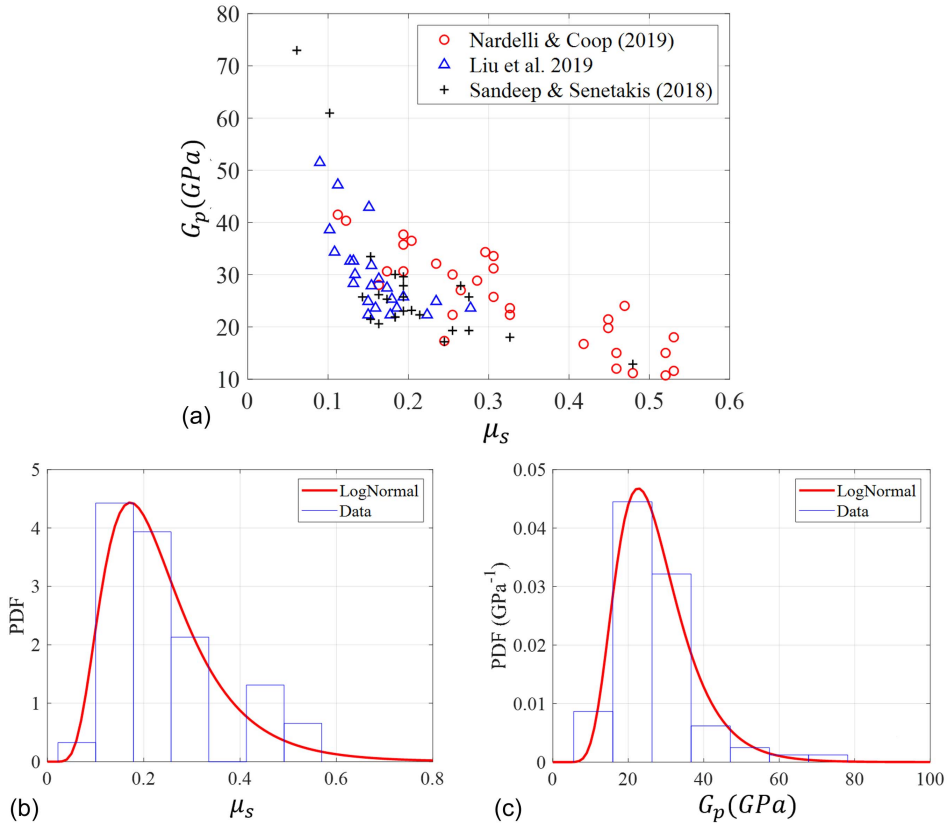

Fig. 2. Probabilistic dependence quantification for μ_s and G_p: (a) collected experimental results; (b) marginal PDF of μ_s; and (c) marginal PDF of G_p.

G_p are known via test data as $\left(\theta_1^{(i)},\ \theta_2^{(i)}\right)$, for $i = 1, \ldots, n$, then the joint PDF of μ_s and G_p can be modeled by the following steps:

1. Determine the marginal PDFs of μ_s and G_p, respectively, according to the test data $\theta_1^{(i)}$ and $\theta_2^{(i)}$, for $i = 1, \ldots, n$, by the maximum likelihood estimation (MLE) with several alternative parametric PDF models. The details can be found in Liu and Lyu (2025).
2. Choose m alternative copula density functions denoted as $c^{(k)}(\cdot, \cdot; \boldsymbol{\lambda}^{(k)})$, for $k = 1, \ldots, m$, where $\boldsymbol{\lambda}^{(k)}$ is the $s^{(k)}$-dimensional undetermined parameter vector.
3. Determine the copula function between μ_s and G_p according to the observed samples $\left(\theta_1^{(i)},\ \theta_2^{(i)}\right)$, for $i = 1, \ldots, n$. Specifically, for each $k = 1, \ldots, m$, the optimal parameter vector $\boldsymbol{\lambda}^{(k)}$ can be given by the MLE, namely, solving the following $s^{(k)}$-dimensional nonlinear equations (Nelsen 2006):

$$\frac{\partial}{\partial \boldsymbol{\lambda}^{(k)}} \sum_{i=1}^{n} \ln c^{(k)}\left(F_1^{(i)}, F_2^{(i)}; \boldsymbol{\lambda}^{(k)}\right) = \mathbf{0}_{s^{(k)}} \tag{2}$$

where

$$F_1^{(i)} = \frac{1}{n}\sum_{j=1}^{n} u\left(\theta_1^{(i)} - \theta_1^{(j)}\right) \quad \text{and} \quad F_2^{(i)} = \frac{1}{n}\sum_{j=1}^{n} u\left(\theta_2^{(i)} - \theta_2^{(j)}\right) \tag{3}$$

in which $u(\cdot)$ = Heaviside's unit step function.

4. Cramer–von Mises test based on Rosenblatt's transform (Genest et al. 2009). For each $k = 1, \ldots, m$, the most common index can be calculated as

$$P^{(k)} = \frac{1}{N}\sum_{l=1}^{N} \mathrm{I}\{S\{z_{1,i}^{(l)}, z_{2,i}^{(l)}; i = 1, \ldots, n\} > S\{F_1^{(i)}, C_{2|1}^{(k)}(F_2^{(i)}|F_1^{(i)}; \boldsymbol{\lambda}^{(k)}); i = 1, \ldots, n\}\} \tag{4}$$

where N = number of the test samples; $\mathrm{I}\{\cdot\}$ = indicative functional; and

$$S\{z_{1,i}, z_{2,i}; i = 1, \ldots, n\} = \frac{n}{9} - \frac{1}{2}\sum_{i=1}^{n}(1 - z_{1,i}^2)(1 - z_{2,i}^2) + \frac{1}{n}\sum_{i=1}^{n}\prod_{j=1}^{n}(1 - \max\{z_{1,i}, z_{1,j}\})(1 - \max\{z_{2,i}, z_{2,j}\}) \tag{5}$$

and $z_{1,i}^{(l)}$ and $z_{2,i}^{(l)}$, for $i = 1, \ldots, n$, are the lth sampling of the $2n$-dimensional independent uniformly distributed variables in [0, 1]; and $C_{2|1}^{(k)}(\cdot \mid \cdot; \boldsymbol{\lambda}^{(k)})$ = corresponding conditional copula function. If $P^{(k)} > 0.05$, then the alternative copula $c^{(k)}(\cdot, \cdot; \boldsymbol{\lambda}^{(k)})$ is accepted; otherwise, it is rejected.

5. For each accepted copula, calculate the Akaike information criterion (AIC) by (Nelsen 2006)

$$AIC^{(k)} = -2\sum_{i=1}^{n} \ln c^{(k)}(F_1^{(i)}, F_2^{(i)}; \boldsymbol{\lambda}^{(k)}) + 2s^{(k)} \tag{6}$$

The copula with the smallest AIC is selected as the optimal model.

These steps enable realistic modeling of the nonlinear coupling between particle-scale properties, preserving the physical interdependencies observed in granular materials. In this study,

Table 1. Performance of alternative copulas

Property	Distribution	Optimal parameters		Kolmogorov–Smirnov statistics
		r	σ	$\alpha = 0.05$; $[D_n^{(\alpha)}] = 0.140$
μ_s	Lognormal	$r = 0.214$	$\sigma = 0.469$	0.123
G_p (GPa)	Lognormal	$r = 25.7$ GPa	$\sigma = 0.354$	0.102

both μ_s and G_p were modeled using lognormal distributions, selected based on Kolmogorov–Smirnov tests and AIC (Ang 2006; Liu and Lyu 2025) [Figs. 2(b and c)]. Table 1 presents their optimal parameters chosen for the study. Subsequently, various copulas, such as Gaussian, student's t-, Frank, and Plackett copulas, were assessed to construct multivariate distribution functions with the specified marginal distributions. Optimal parameters and corresponding AIC values for these copulas were determined, with further details provided in a later section.

Computational Mechanical Analysis Via the Discrete-Element Method

In the DEM simulations, deterministic particle properties such as μ_s, G_p, and υ were used to determine outputs such as force and stress in specimens under specified conditions, illustrating the relationship between particle-scale inputs and macroscale soil behavior. The simulations were conducted using a modified version of LAMMPS (Large-Scale Atomic / Molecular Massively Parallel Simulator) (Thompson et al. 2022), employing cubic samples with periodic boundaries and no gravitational forces (Thornton 2000). Particles were modeled as spheres to eliminate shape effects (Zhao et al. 2023) and assigned a density of 2,670 kg/m^3 (Barreto 2008). Specimen generation involved randomly distributing grains in noncontact configurations using a custom algorithm.

The Hertz–Mindlin contact model was adopted to investigate the uncertainties in μ_s and G_p, with υ fixed at 0.2 due to the difficulty of directly measuring υ in experimental studies. 100 representative data were generated based on the established model, incorporating the coupled and dependent effects of μ_s and G_p, as shown in Fig. 3(c), employed as representative input parameters for the subsequent numerical simulations.

Specimens were isotopically compressed to a mean effective stress of 100 kPa, following the methodology proposed by Cundall (1988). Equilibrium was confirmed when the coordination number (Z) stabilized, with fluctuations below 0.001 after 500,000 simulation cycles. To capture the state-dependent behavior of granular materials, three packing densities were considered, controlled by the initial interparticle friction coefficients (μ_{iso}) during the isotropic compression stage, set at 0.001, 0.04, and 0.1, respectively. After compression, the isotropic friction coefficient (μ_{iso}) of each specimen was replaced with its corresponding μ_s values to reestablish equilibrium, enabling subsequent drained triaxial shear simulations. Recognizing the importance of both small- and large-strain soil behavior, a total of 600 simulations were performed: 300 focused on large-strain behavior approaching the critical soil state, and the remaining 300 examined small-strain behavior.

Probability Density Evolution of Mechanical Behavior

The propagation of uncertainties in particle-scale properties to macroscale behavioral outcomes can be effectively analyzed using the PDEM framework. A brief overview of this approach is provided subsequently. Macroscale soil behaviors, including the stress ratio (η) and void ratio (e), etc., are directly affected by uncertainties

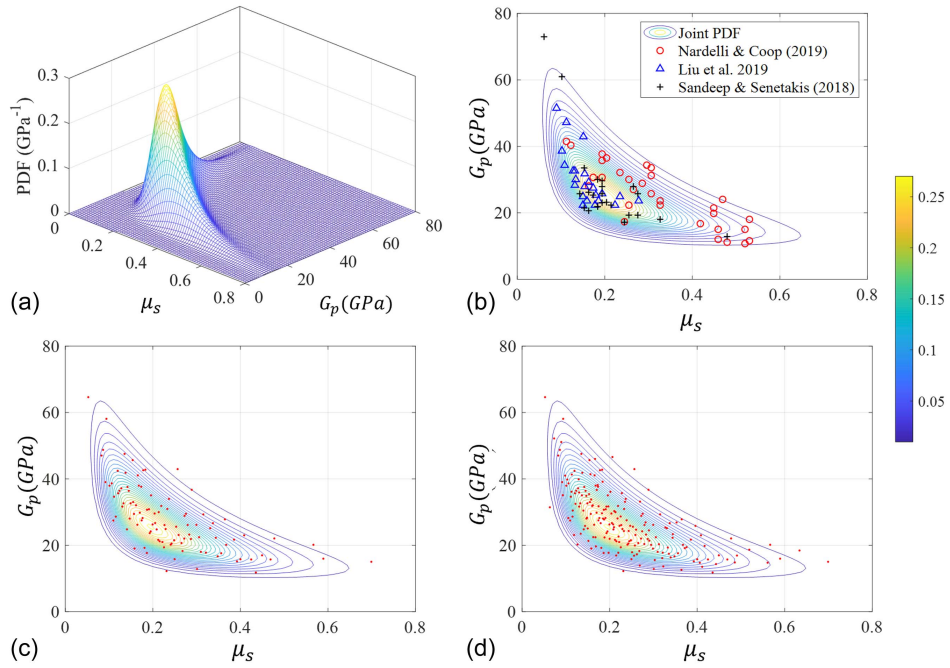

Fig. 3. Full probability quantification for particle properties of μ_s and G_p: (a) 3D PDF profiles; (b) joint PDF for μ_s and G_p; (c) 100 representative points; and (d) 200 representative points.

at the particle scale. This relationship can be mathematically expressed as

$$X = h(\boldsymbol{\Theta}, \varepsilon) \tag{7}$$

In this analysis, X = macroscale soil behavior metric, such as the stress ratio (η), void ratio (e), or coordination number (Z); while $\boldsymbol{\Theta}$ = particle-scale properties (i.e., μ_s and G_p). The mapping of these particle-scale inputs to macroscale outputs is governed by the deterministic function $h(\cdot)$ within the DEM framework. However, due to inherent variability in $\boldsymbol{\Theta}$, these properties are better represented as random variables (Liu and Lyu 2023b; Liu et al. 2024b). Consequently, X becomes a stochastic process that evolves with axial strain (ε). To quantify this uncertainty propagation, the PDEM framework is applied, enabling a detailed analysis of how the probabilistic characteristics of $\boldsymbol{\Theta}$ influence X over the strain domain. This stochastic behavior of X is inherently driven by the uncertainties embedded in $\boldsymbol{\Theta}$.

A specific instance of $X(\varepsilon)$, expressed as $X(\varepsilon) = h(\boldsymbol{\Theta}, \varepsilon)$, can be determined through deterministic DEM simulations for a given realization $\boldsymbol{\Theta} = \boldsymbol{\theta}$. However, performing numerous stochastic simulations to account for the variability in $X(\varepsilon)$ is computationally infeasible due to the intensive demands of DEM. To overcome this limitation, the PDEM framework is employed. It efficiently tracks the evolution of the PDF, capturing the system's behavior under analogous physical mechanisms without the need for extensive computational resources.

The PDEM framework provides two key advantages: (1) it directly computes the PDF of the targeted macroscale behavior; and (2) it significantly reduces computational costs, enabling the practical implementation of stochastic DEM simulations. The core equation of PDEM, initially proposed by Li and Chen (2008) and later refined by Li and Chen (2008), models the stochastic nature of $X(\varepsilon)$ resulting from uncertainties in $\boldsymbol{\Theta}$. The joint PDF of $X(\varepsilon)$ and $\boldsymbol{\Theta}$, represented as $p_{X\boldsymbol{\Theta}}(x, \boldsymbol{\theta}, \varepsilon)$, is governed by

$$\frac{\partial p_{X\boldsymbol{\Theta}}(x, \boldsymbol{\theta}, \varepsilon)}{\partial \varepsilon} + \frac{\partial h(\boldsymbol{\theta}, \varepsilon)}{\partial \varepsilon} \frac{\partial p_{X\boldsymbol{\Theta}}(x, \boldsymbol{\theta}, \varepsilon)}{\partial x} = 0 \tag{8}$$

with the initial condition

$$p_{X\boldsymbol{\Theta}}(x, \boldsymbol{\theta}, 0) = \delta(x - x_0) p_{\boldsymbol{\Theta}}(\boldsymbol{\theta}) \tag{9}$$

where $\delta(\cdot)$ = Dirac's delta function; x_0 = initial value of X when $\varepsilon = 0$; and $p_{\boldsymbol{\Theta}}(\boldsymbol{\theta})$ = PDF of $\boldsymbol{\Theta}$ modeled in the "Probabilistic Dependence Quantification of Particle Properties." Then the PDF of $X(\varepsilon)$, denoted as $p_X(x, \varepsilon)$ is given by

$$p_X(x, \varepsilon) = \int_{\Omega_{\boldsymbol{\Theta}}} p_{X\boldsymbol{\Theta}}(x, \boldsymbol{\theta}, \varepsilon) \mathrm{d}\boldsymbol{\theta} \tag{10}$$

where $\Omega_{\boldsymbol{\Theta}}$ = distribution domain of $\boldsymbol{\Theta}$.

Eq. (8), referred to as the generalized density evolution equation (GDEE) or Li-Chen equation in some references (e.g., Nielsen et al. 2016), serves as the cornerstone of the PDEM framework. Originally proposed by Li and Chen (2008), it is grounded in the principle of preservation of probability for random event description. Variants of this equation have been utilized in subsequent research (Li et al. 2012; Lyu and Chen 2022), to analyze stochastic systems. The GDEE allows for the characterization of the probability distribution of $X(\varepsilon)$ by solving it within the PDEM framework, provided the deterministic function $h(\cdot)$ is well-defined for each realization of $\boldsymbol{\Theta}$.

The implementation methodologies of PDEM, including its practical algorithms, have been thoroughly documented in the literature (Hai and Lyu 2023; Lyu et al. 2024e). By assuming that $h(\boldsymbol{\Theta}, \varepsilon)$ is approximately equal to $h(\boldsymbol{\theta}_q, \varepsilon)$ within each subdomain Ω_q for $q = 1, \ldots, n_{\text{sel}}$, the GDEE can be reformulated to accommodate these discrete intervals. This reformulation simplifies numerical computation and is expressed as Liu and Lyu (2025)

$$\frac{\partial p_X^{(q)}(x, \varepsilon)}{\partial \varepsilon} + \frac{\partial h(\boldsymbol{\theta}_q, \varepsilon)}{\partial \varepsilon} \frac{\partial p_X^{(q)}(x, \varepsilon)}{\partial x} = 0, \quad \text{for } q = 1, \ldots, n_{\text{sel}} \tag{11}$$

by integrating Eq. (8) over Ω_q with respect to $\boldsymbol{\Theta}$, where

$$p_X^{(q)}(x, \varepsilon) = \int_{\Omega_q} p_{X\boldsymbol{\Theta}}(x, \boldsymbol{\theta}, \varepsilon) \mathrm{d}\boldsymbol{\theta}, \quad \text{for } q = 1, \ldots, n_{\text{sel}} \tag{12}$$

Simultaneously, the initial condition of Eq. (11) can be given as

$$p_X^{(q)}(x, 0) = \delta(x - x_0) P_q, \quad \text{for } q = 1, \ldots, n_{\text{sel}} \tag{13}$$

Referring to Eqs. (8) and (11), the latter represents a hyperbolic partial differential equation (PDE) that can be solved using various numerical techniques. A particularly effective method is the finite-difference method combined with the total variation diminishing (TVD) scheme, as described by Li and Chen (2009). The full algorithm for solving the GDEE to obtain the transient PDF of the mechanical response of granular materials using the TVD scheme is detailed in Liu and Lyu (2023b). Following this step, the PDF of $X(\varepsilon)$ must be computed. Consistent with Eqs. (10) and (12), the PDF of $X(\varepsilon)$ is determined by

$$p_X(x, \varepsilon) = \sum_{q=1}^{n_{\text{sel}}} p_X^{(q)}(x, \varepsilon) \tag{14}$$

A comprehensive understanding of macroscale soil behavior requires the detailed characterization of PDFs for specific behavioral metrics. By leveraging PDFs for granular material properties instead of relying solely on mean values, the accuracy of stochastic mechanical behavior analysis is significantly improved. This approach captures the inherent variability of granular materials with accuracy comparable to deterministic methods, while realistically modeling particle-scale heterogeneity. By integrating advanced stochastic algorithms with DEM, the framework reveals detailed micro-to-macro mechanical behavior, including probability density distributions and statistical moments. Besides, analyzing the propagation of uncertainty and the resulting PDFs for individual behavioral metrics in isolation may overlook the inherent coupling and interdependencies among these metrics. For instance, the uncertainty in stress ratios with increasing axial strain could be closely correlated with uncertainties in void ratio or coordination number. To address these interdependencies effectively, the decoupled M-PDEM approach proposed by Lyu et al. (2024e) provides a framework for capturing and analyzing these complex relationships.

Without loss of generality, if the joint distribution of two probabilistically dependent response quantities, X_1 and X_2, is of interest, these quantities can be expressed as functions of the basic random variable $\boldsymbol{\Theta}$ and evaluation strain ε, such that $X_1(\varepsilon) = h_1(\boldsymbol{\Theta}, \varepsilon)$ and $X_2(\varepsilon) = h_2(\boldsymbol{\Theta}, \varepsilon)$, following the principle of probability preservation. Using the decoupled M-PDEM framework, the joint PDF of X_1 and X_2 can then be formulated as Lyu et al. (2024e)

$$\begin{aligned} p_{X_1X_2}(x_1, x_2, \varepsilon) &= \int_{\Omega_{\boldsymbol{\Theta}}} p_{X_1X_2\boldsymbol{\Theta}}(x_1, x_2, \boldsymbol{\theta}, \varepsilon) \mathrm{d}\boldsymbol{\theta} \\ &= \int_{\Omega_{\boldsymbol{\Theta}}} \frac{p_{X_1\boldsymbol{\Theta}}(x_1, \boldsymbol{\theta}, \varepsilon) p_{X_2\boldsymbol{\Theta}}(x_2, \boldsymbol{\theta}, \varepsilon)}{p_{\boldsymbol{\Theta}}(\boldsymbol{\theta})} \mathrm{d}\boldsymbol{\theta} \end{aligned} \tag{15}$$

where $p_{X_1\boldsymbol{\Theta}}(x_1,\boldsymbol{\theta},\varepsilon)$ and $p_{X_2\boldsymbol{\Theta}}(x_2,\boldsymbol{\theta},\varepsilon)$ can be calculated respectively by the GDEE [e.g., Eq. (8)], namely,

$$\frac{\partial p_{X_1\boldsymbol{\Theta}}(x_1,\boldsymbol{\theta},\varepsilon)}{\partial\varepsilon}+\frac{\partial h_1(\boldsymbol{\theta},\varepsilon)}{\partial\varepsilon}\frac{\partial p_{X_1\boldsymbol{\Theta}}(x_1,\boldsymbol{\theta},\varepsilon)}{\partial x_1}=0,$$
$$\frac{\partial p_{X_2\boldsymbol{\Theta}}(x_2,\boldsymbol{\theta},\varepsilon)}{\partial\varepsilon}+\frac{\partial h_2(\boldsymbol{\theta},\varepsilon)}{\partial\varepsilon}\frac{\partial p_{X_2\boldsymbol{\Theta}}(x_2,\boldsymbol{\theta},\varepsilon)}{\partial x_2}=0 \quad (16)$$

Eq. (15) separates the joint PDF of probabilistically dependent responses into the individual PDFs of each response, described within the framework of random events. This decoupling allows each response to be governed independently by its respective one-dimensional PDE.

The specific implementation for capturing the joint PDF via the decoupled M-PDEM is as follows:

1. Probability Space Partition: An appropriate numerical method (e.g., Chen and Zhang 2013; Chen et al. 2016, 2024) is employed to generate n_{sel} representative points, $\boldsymbol{\theta}^{(q)}$ $(q=1,\ldots,n_{\text{sel}})$, for the basic random variables $\boldsymbol{\Theta}$. The probability associated with each representative point, P_q $(q=1,\ldots,n_{\text{sel}})$, is then calculated.
2. DEM Analysis: For each representative point $\boldsymbol{\theta}^{(q)}$ $(q=1,\ldots,n_{\text{sel}})$, DEM simulations are performed to obtain the numerical solutions $X_1(\varepsilon)=h_1(\boldsymbol{\theta}^{(q)},\varepsilon)$ and $X_2(\varepsilon)=h_2(\boldsymbol{\theta}^{(q)},\varepsilon)$ (e.g., Liu and Lyu 2023b, 2025).
3. Numerical Solution of the GDEE: For each representative point $\boldsymbol{\theta}^{(q)}$ $(=1,\ldots,n_{\text{sel}})$, substitute $X_1(\varepsilon)=h_1(\boldsymbol{\theta}^{(q)},\varepsilon)$ and $X_2(\varepsilon)=h_2(\boldsymbol{\theta}^{(q)},\varepsilon)$, into Eqs. (16). Solve the equation numerically under the specified initial conditions using appropriate numerical methods (e.g., Wang and Li, 2020; Lyu et al. 2024a).
4. Transformation to the Joint Dependence PDF: Derive the joint PDF $p_{X_1X_2}(x_1,x_2,\varepsilon)$ by combining the decoupled marginal solutions. This involves performing a multidimensional integration as specified in Eq. (15).

Results and Discussion

Full Probability Quantification of Extensive Experimental Data

As previously analyzed, comprehensive experimental data from earlier studies revealed a distinct nonlinear relationship between μ_s and G_p, as depicted in Fig. 2(a). The data presented that higher μ_s values corresponded to lower G_p values, and vice versa.

To realistically capture the coupling between particle-scale properties, four copula models—Gaussian, student's t-, Frank, and Plackett—were evaluated for their suitability in representing the observed dependencies. The models were optimized, with the key results summarized in Table 2. The three-dimensional (3D) fit and two-dimensional projections of the optimized PDFs derived from the experimental data are illustrated in Figs. 3(a and b), respectively. Additionally, representative samples of 100 and 200 points are depicted in Figs. 3(c and d). For this study, a set of 100 representative points was selected to achieve a balance between computational efficiency and accuracy.

Table 2. Performance of alternative copulas

Alternative copulas	Optimal parameters	AIC
Gaussian	$\lambda=-0.738$	−59.25
Student's t-test	$\lambda_1=-0.722$; $\lambda_2=6.05$	−57.94
Frank	$\lambda=-5.40$	−43.68
Plackett	$\lambda=0.198$	−41.78

The Gaussian copula was determined to be the most appropriate PDF for describing the coupled particle properties, as evaluated using the Kolmogorov–Smirnov test and the AIC, following the guidelines proposed by Ang (2006). The criteria included a significance level of 0.05 and a Kolmogorov–Smirnov critical value of 0.140. This model provided a superior fit, generating 100 representative points with μ_s values ranging from approximately 0.15 to 0.65 and G_p values between 16 and 61 GPa. The simulations were then conducted using a relatively uniform PSD, illustrated in Fig. 4. This PSD, commonly used in numerical studies (e.g., Huang 2014), effectively restricts PSD-related influences, making it appropriate for isolating the effects of particle-scale parameters in preliminary uncertainty analyses (e.g., Liu et al. 2023). Note that all samples share the same particle assembly, with identical size distribution and particle count. Each numerical sample contained 23,312 particles, ensuring sufficient representativeness for deterministic DEM analyses. The Hertz–Mindlin contact model was employed, with no damping ratio incorporated. The simulation process included an initial isotropic compression phase, followed by drained shearing simulations.

The simulations were conducted in two stages: isotropic compression followed by a shearing phase. Adopting the approach of Liu et al. (2021), three distinct densities were achieved by varying the interparticle friction coefficient (μ_{iso}) during isotropic compression, set at 0.001, 0.04, and 0.1, while maintaining particle shear modulus (G_p) values corresponding to the generated representative points. This setup resulted in approximately 300 simulations for the consolidation phase. While previous studies (i.e., Liu and Lyu 2025) have indicated that property uncertainty in G_p has a negligible influence on the initial soil state prior to shearing, this study also quantified the initial soil state to ensure a thorough and consistent analysis. The primary characteristics of the specimens following the isotropic compression stage were analyzed and are detailed in Table 3. The findings reveal that initial soil states exhibit minimal uncertainty for the same μ_{iso} values, as evidenced by the low coefficients of variation (COVs) for these key parameters (i.e., e, e_m, Z, and Z_m) provided in Table 3. For the subsequent shearing phase, 100 simulations were performed for each density level to examine uncertainties across both small-strain and

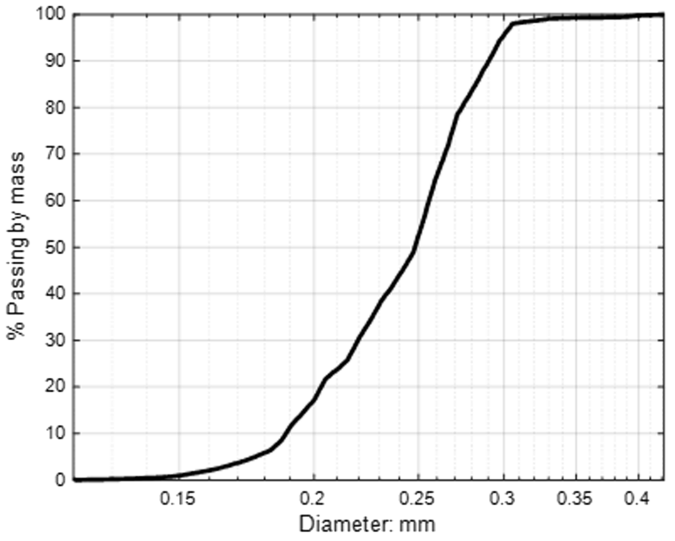

Fig. 4. PSD of simulated specimens in DEM.

Table 3. Initial soil state before shearing

	$\mu_{iso} = 0.001$		$\mu_{iso} = 0.04$		$\mu_{iso} = 0.1$	
Property	Mean	COV	Mean	COV	Mean	COV
e	0.538	0.001	0.582	0.007	0.620	0.005
e_m	0.581	0.004	0.642	0.011	0.705	0.008
Z	5.77	0.006	5.33	0.010	4.92	0.008
Z_m	6.14	0.004	5.76	0.007	5.43	0.005

large-strain behaviors, resulting in a total of 600 simulation cases in this study.

To ensure quasi-static conditions during the tests, the shearing velocity was carefully controlled so that the inertia number (I) remained approximately 1×10^{-4}, significantly below the threshold value of 2.5×10^{-3} recommended by Da Cruz et al. (2005). The inertia number was computed using the formula $I = \dot{\varepsilon} d_{50} \sqrt{\rho / p'}$, where $\dot{\varepsilon}$ represents the strain rate, d_{50} is the median particle diameter (0.248 mm), ρ is the particle density (2,670 kg/m^3), and p' denotes the mean effective stress (100 kPa).

Results of Comprehensive Granular Material Behavior

This study aims to enhance the realistic modeling of granular materials by capturing the coupled variability of key particle-scale properties and their influence on macroscopic behavior. It focuses on how these particle-scale property uncertainties influence macroscale responses, including the stress ratio, void ratio, coordination number, small-strain stiffness, stress transmission, etc., as axial strain increases. Firstly, the stress ratio (q/p') is a key macroscale parameter directly linked to the friction angle and widely used in geotechnical design. Here, q is the deviatoric stress, defined as $q = (\sigma_1 - \sigma_3)$, where σ_1 and σ_3 are the major and minor principal stresses from drained triaxial tests. The mean effective stress is calculated as $p' = (\sigma_1 + 2\sigma_3)/3$. Analyzing the evolution of q/p' with axial strain provides critical insights into the macroscopic mechanical behavior of granular materials relevant to engineering applications.

The PDF of stress ratios provides a detailed depiction of granular material behavior as axial strain develops. As illustrated in Fig. 5(a), the PDF contours of stress ratios consolidate results from multiple simulations, capturing the response across three distinct packing densities. This representation enables a more realistic modeling of the inherent coupling between particle-scale properties and their impact on macroscopic soil behavior. By reflecting these physically meaningful interactions, it allows engineers to identify critical response ranges, including "best-case" and "worst-case" scenarios. The evolution of these PDFs provides a robust link between microscale heterogeneity and macroscale performance, supporting reliability analysis, risk evaluation, and sensitivity studies in geotechnical engineering. The results also demonstrate that, by realistically capturing the coupled effects of μ_s and G_p, the macroscale responses—such as the stress ratio, void ratio, and volumetric strain—stabilize toward characteristic critical state values at axial strains beyond 25% during sustained shearing.

For comparison, Fig. 5(b) presents the PDF contours of stress ratios as axial strain increases, accounting solely for the uncertainty in G_p while keeping μ_s fixed at 0.25 (i.e., average value). The results present that the individual variability of G_p has limited influence on large-strain behavior. However, its coupling with μ_s induces notable effects on macroscopic responses, highlighting the importance of capturing interparameter dependencies for realistic modeling of granular materials. Meanwhile, Fig. 5(c) presents the evolution of mean stress ratio values with axial strain for three different packing densities. The gray envelope surrounding the mean curve represents the range within ± two standard deviations, illustrating the variability. These results also verify that stress ratios reach a stable state beyond an axial strain of approximately 25%, marking the onset of critical soil states.

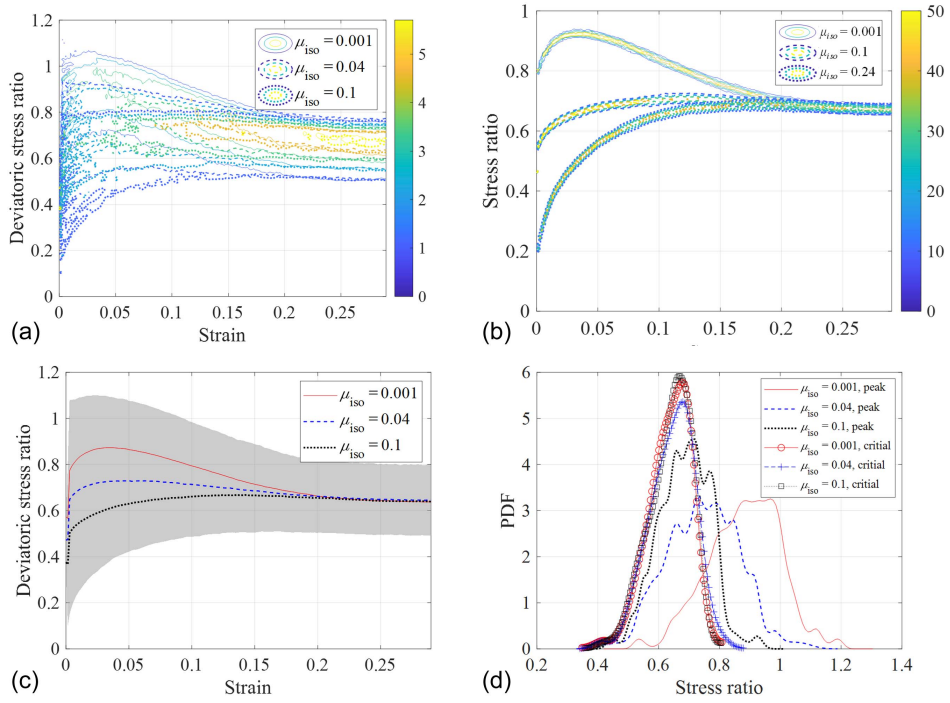

Fig. 5. Comprehensive behavior of stress ratios: (a) PDF contours (uncertainty of coupled μ_s and G_p); (b) PDF contours (uncertainty of G_p); (c) mean stress ratios curves; and (d) PDF of stress ratios under peak and critical soil states.

J. Geotech. Geoenviron. Eng., 2026, 152(2): 04025181

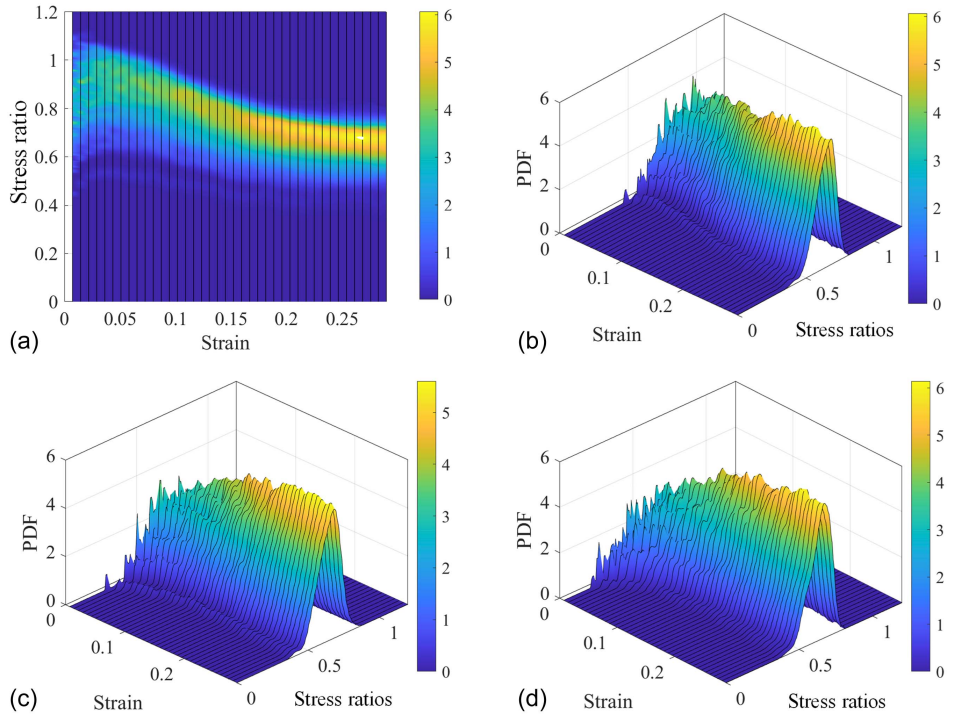

Fig. 6. 3D PDF surfaces with varying initial states: (a) μ_{iso} of 0.001 in plane view; (b) μ_{iso} of 0.001; (c) μ_{iso} of 0.04; and (d) μ_{iso} of 0.1.

Fig. 5(d) then highlights two critical soil states: the peak state, characterized by the maximum stress ratio, and the critical soil state. The results demonstrate that the propagation of uncertainties from coupled particle-scale properties to stress ratios is significantly influenced by soil states and packing densities. Notably, the PDF of stress ratios at the peak state exhibits considerable variability across different packing densities. For instance, when $\mu_{iso} = 0.001$, stress ratios range from approximately 0.6 to 1.2, whereas for $\mu_{iso} = 0.1$, the range narrows to approximately 0.5 to 0.9. In contrast, at the critical state, the PDF profiles are nearly identical across all packing densities, displaying consistent mean values and COVs within the range of approximately 0.5 to 0.8. This consistency reflects fundamental principles of soil mechanics, underscoring the inherent stability and reproducibility of critical states. Fig. 6 then illustrates the 3D PDF surfaces, capturing the evolution of stress ratios with axial strain across varying packing densities. This visualization provides a valuable tool for engineering applications by offering an intuitive representation of the probabilistic soil response. Specifically, Figs. 6(a and b) present the results for $\mu_{iso} = 0.001$, shown in a planar and 3D perspective, respectively. Similarly, Figs. 6(c and d) depict the 3D PDF surfaces for $\mu_{iso} = 0.04$ and 0.1, respectively.

Beyond assessing stress ratio responses under realistically modeled particle-scale variability, this study also examines the void ratio response as axial strain develops. As presented in Fig. 7, the data points corresponding to both peak and critical stress ratios were identified to examine the evolution of void ratio with increasing axial strain. The results in Fig. 8 indicate that void ratio responses, like that of stress ratios, is also significant. Specifically, Fig. 8(a) illustrates the PDF contours for void ratio, reflecting how the inherent coupling between particle-scale properties influences volumetric behavior across different densities. While previous studies have presented that uncertainty in G_p alone has a negligible impact on void ratio evolution with increasing axial strain, the coupled interaction of μ_s and G_p significantly alters this response. This underscores the necessity of realistically capturing particle-scale properties dependencies to represent the compressibility and dilatancy behavior of granular materials with physical fidelity. Fig. 8(b) demonstrates that void ratio PDFs exhibit considerable variability at peak stress ratio points across different densities. However, this variability diminishes at the critical state, where the void ratio PDF profiles converge, again reflecting the inherent consistency of soil properties at critical states. Furthermore, Figs. 8(c and d) depict the 3D PDF surfaces for $\mu_{iso} = 0.001$ and 0.1, respectively, consistently demonstrating a similar range of void ratios at the critical state.

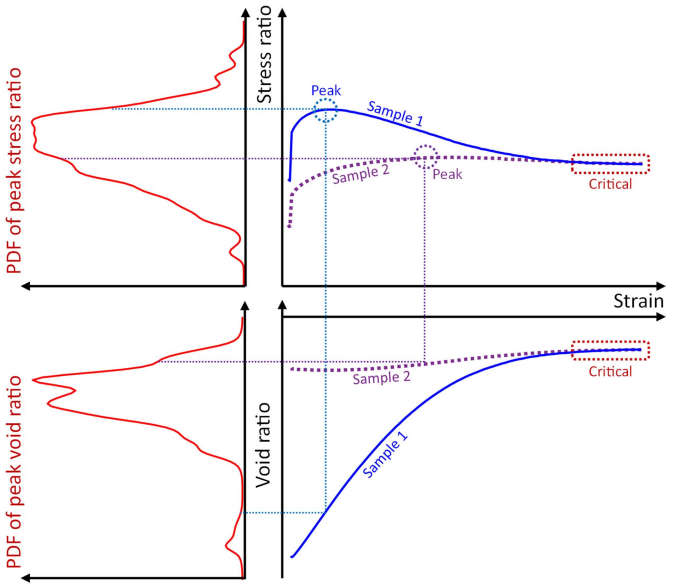

Fig. 7. Quantification of peak and critical soil state of both the stress ratios and void ratios with increasing axial strain.

J. Geotech. Geoenviron. Eng., 2026, 152(2): 04025181

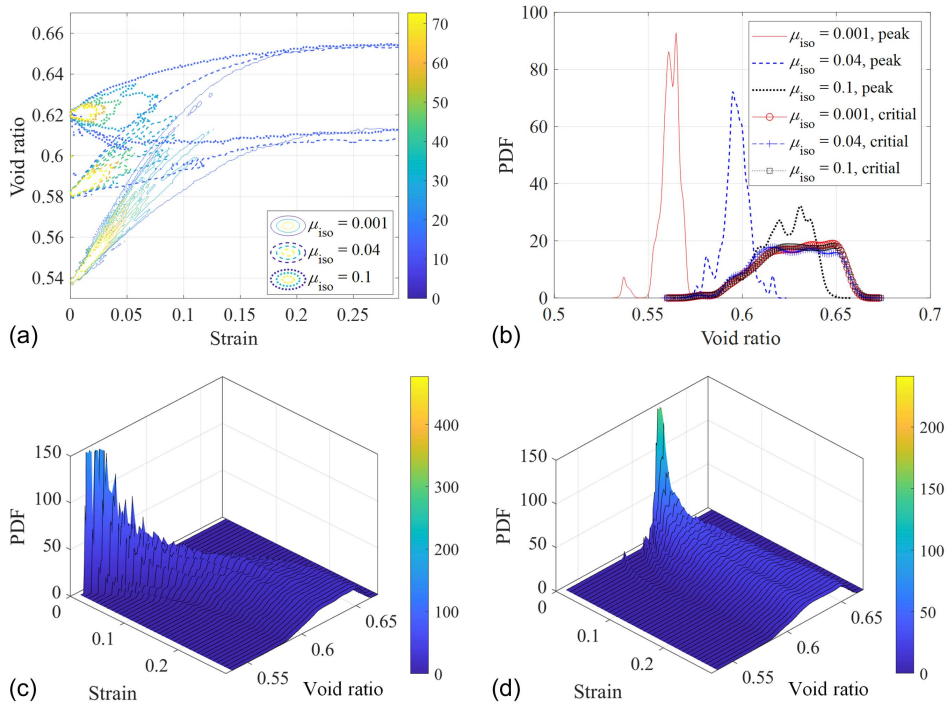

Fig. 8. Comprehensive behavior of void ratios with increasing axial strain: (a) PDF contours; (b) PDF obtained in both peak and critical soil states; (c) 3D PDF surfaces with μ_{iso} of 0.001; and (d) 3D PDF surfaces with μ_{iso} of 0.1.

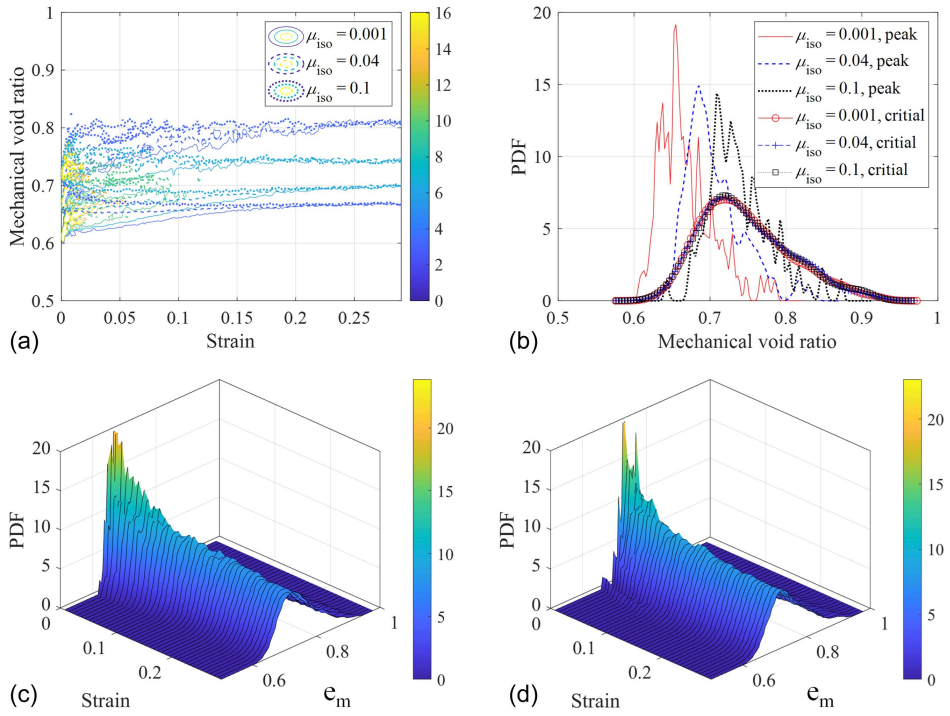

Fig. 9. Comprehensive behavior of mechanical void ratios with increasing axial strain: (a) PDF contours; (b) PDF obtained in both peak and critical soil states; (c) 3D PDF surfaces with μ_{iso} of 0.001; and (d) 3D PDF surfaces with μ_{iso} of 0.1.

A key advantage of the DEM is its capacity to analyze the behavior of individual particles and contact points, offering insights that surpass those obtained through traditional experimental techniques. Previous studies have demonstrated that the mechanical void ratio (e_m), which considers inactive particles as part of the void space, provides more accurate predictions of soil behavior compared to the conventional global void ratio (e). Fig. 9(a) then highlights the propagated uncertainty of e_m with increasing axial strain, revealing its strong dependence on the soil state. Fig. 9(b) presents the PDF profiles for different packing densities at both peak stress ratio points and critical states. While the PDF curves differ significantly at peak stress ratios, they

J. Geotech. Geoenviron. Eng., 2026, 152(2): 04025181

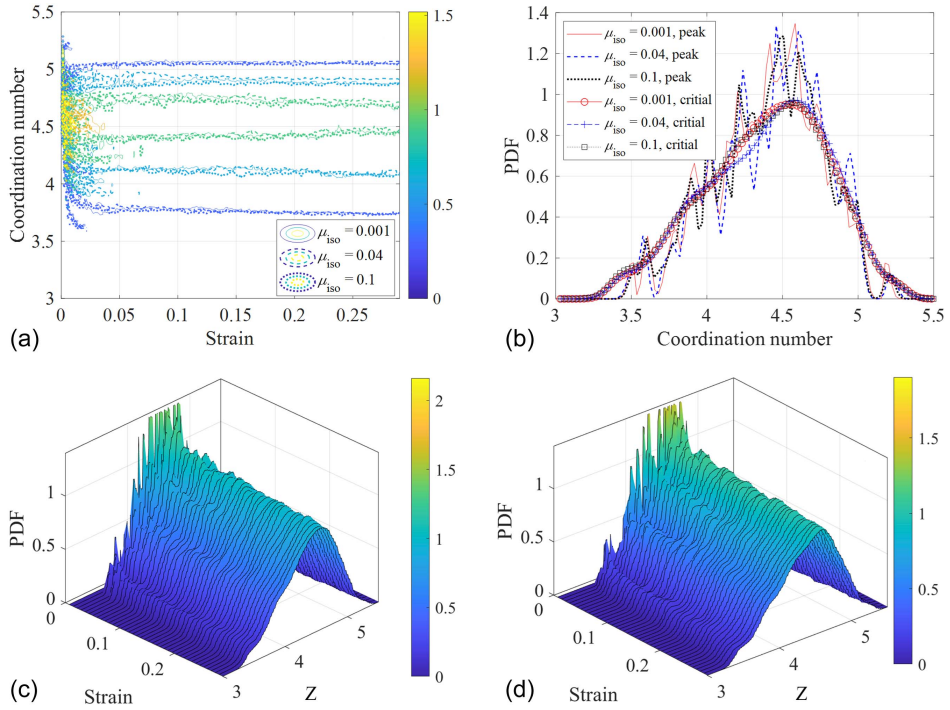

Fig. 10. Comprehensive behavior of coordination number with increasing axial strain: (a) PDF contours; (b) PDF obtained in both peak and critical soil states; (c) 3D PDF surfaces with μ_{iso} of 0.001; and (d) 3D PDF surfaces with μ_{iso} of 0.1.

converge at the critical state, consistent with principles of critical state soil mechanics. Additionally, Figs. 9(c and d) present the 3D PDF profiles for cases with $\mu_{iso} = 0.001$ and 0.1, respectively, offering valuable insights for predicting realistic packing density distributions.

Fig. 10 examines the propagation of uncertainties in coordination number (Z), a key parameter for evaluating the mechanical stability and structural integrity of soil at the microscale. Additionally, Z serves as an essential metric for estimating the small-strain stiffness (G_p) of the specimens, which is a critical consideration in practical engineering design. Consistent with trends observed in stress ratio and void ratio, the coordination number (Z) is also strongly influenced by the coupled particle properties between μ_s and G_p. However, unlike the trends observed for stress and void ratios, the uncertainty in Z is largely independent of packing density and soil state. Fig. 10(b) shows that the PDF profiles for Z remain consistent across different packing densities and soil states, with values ranging from approximately 3.3 to 5.5. This stability can likely be attributed to the relatively uniform PSD used in this study, which allows Z values to quickly stabilize as axial strain increases. Figs. 10(c and d) further illustrate the 3D PDF profiles of Z for $\mu_{iso} = 0.001$ and 0.1, respectively. The uncertainty in the mechanical coordination number (Z_m) was also analyzed, excluding inactive particles in its calculation, consistent with the approach for the mechanical void ratio (e_m). As presented in Fig. 11, the uncertainty patterns for Z_m closely mirror those observed for Z, with negligible influence from initial packing densities or soil states. This is evident from the nearly identical PDF profiles across different densities at both critical and peak soil states. Furthermore, the 3D PDF surfaces in Figs. 11(c and d), representing $\mu_{iso} = 0.001$ and 0.1, respectively, also exhibit convergence, reinforcing this observation.

The anisotropic properties of granular materials during the shearing stage can be significant and are effectively captured in the DEM using the fabric tensor, Φ, defined as

$$\Phi_{ij} = \frac{1}{N_c}\sum_{k=1}^{N_c} n_i^{(k)} n_j^{(k)} \tag{17}$$

where $n_i^{(k)}$ = contact normal vector for contact k; and N_c = total number of contacts. The deviatoric fabric component of the fabric tensor can be derived as

$$\Phi_{dev} = \Phi_1 - \Phi_3 \tag{18}$$

In this context, Φ_1 and Φ_3 denote the major and minor principal components of the fabric tensor, respectively. The deviatoric component (Φ_{dev}) quantifies soil anisotropy by assessing the preferential alignment of particle contacts, reflecting directional biases within the internal structure of soil specimens, especially in axisymmetric configurations. Fig. 12(a) illustrates the variability in Φ_{dev} with increasing axial strain across different packing densities, emphasizing the influence of packing density and soil state on anisotropy. Fig. 12(b) presents the PDF profiles for peak stress ratio points and critical states across three packing densities. While the PDFs at peak stress ratio points show distinct differences, those at the critical state converge, underscoring the dominant role of critical states over initial density effects. Additionally, Figs. 12(c and d) present the 3D PDF surfaces for $\mu_{iso} = 0.001$ and 0.1, respectively, further validating the effectiveness of quantifying the propagation of uncertainty from coupled particle properties to anisotropy.

In addition to uncertainties associated with large-strain shearing, the behavior of granular materials at small strains can also have a profound impact on macroscale responses. For instance, small-strain stiffness (G_0) is a critical macroscale parameter for predicting settlement and related behaviors. As presented in Fig. 13(a), substantial variability in G_0 values is evident across the three packing densities. These G_0 values are calculated using a small shear probe method, following the procedures described by Kuwano and Jardine (2002) and Liu et al. (2022). In this approach, a shear strain threshold of 1×10^{-5} is used to define the elastic linear range.

J. Geotech. Geoenviron. Eng., 2026, 152(2): 04025181

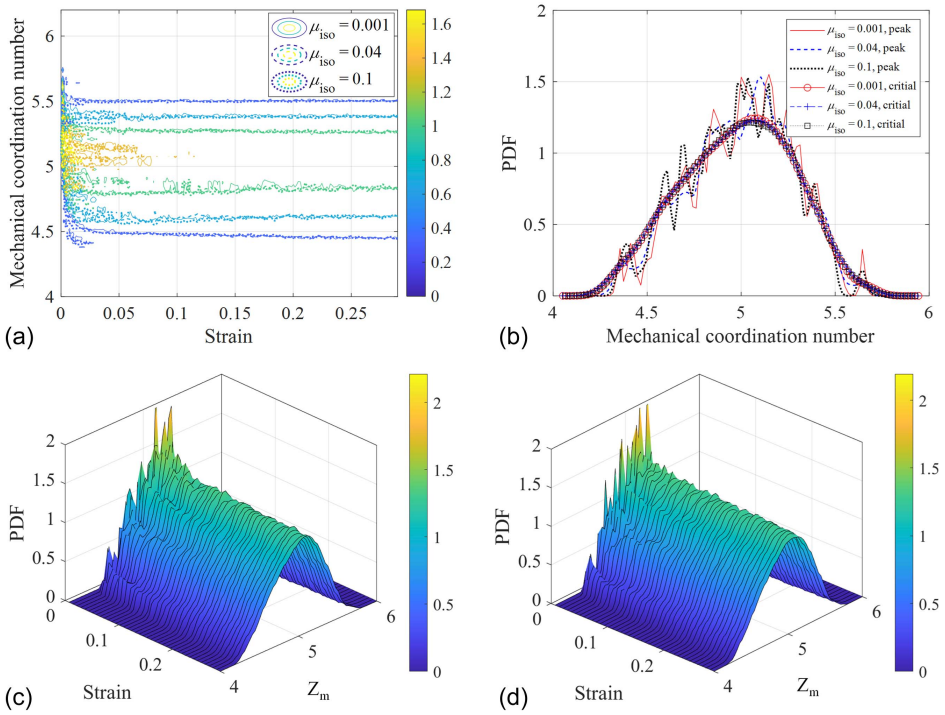

Fig. 11. Comprehensive behavior of mechanical coordination values with increasing axial strain: (a) PDF contours; (b) PDF obtained in both peak and critical soil states; (c) 3D PDF surfaces with μ_{iso} of 0.001; and (d) 3D PDF surfaces with μ_{iso} of 0.1.

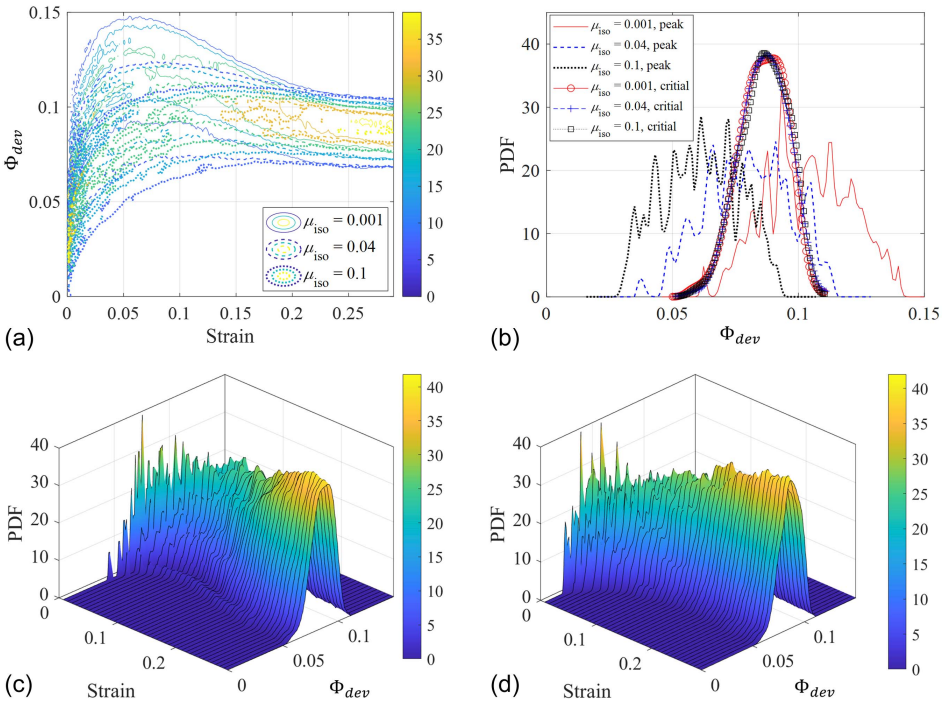

Fig. 12. Comprehensive behavior of anisotropy with increasing axial strain: (a) PDF contours; (b) PDF obtained in both peak and critical soil states; (c) 3D PDF surfaces with μ_{iso} of 0.001; and (d) 3D PDF surfaces with μ_{iso} of 0.1.

Fig. 13(a) highlights the variation in mean G_0 values across different packing densities, showing higher values for dense conditions and lower values for loose conditions. The coupled influence of G_p and μ_s significantly impacts G_0, contributing to notable uncertainty in its values.

Another key parameter related to the peak stress ratio is dilatancy, a critical factor in predicting extreme material behavior. According to Liu and Lourenço (2021), soil dilatancy is defined as $D^p = -d\varepsilon_v^p/d\varepsilon_q^p$, where $d\varepsilon_v^p$ is the increment in plastic volumetric strain, and $d\varepsilon_q^p$ is the increment in plastic deviatoric strain.

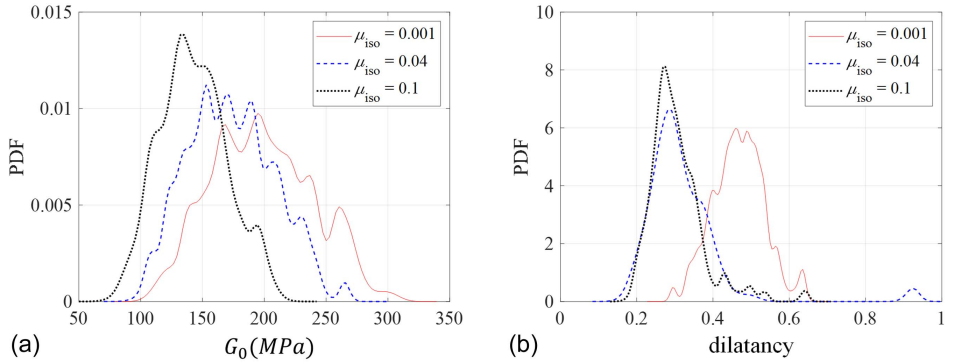

Fig. 13. PDF profiles for small-strain stiffness and shear dilatancy: (a) small-strain stiffness behavior; and (b) dilatancy behavior.

Fig. 13(b) illustrates the uncertainty in D^{p} for the three packing densities corresponding to $\mu_{\mathrm{iso}} = 0.001$, 0.04, and 0.1. The figure reveals distinct PDF variations across densities, emphasizing the role of packing density in influencing soil dilatancy. Notably, D^{p} is closely tied to the peak strength of granular materials and is characterized by the mobilized stress ratio, a vital macroscale parameter.

As highlighted by Liu et al. (2023), the internal stress distribution within each DEM specimen plays a crucial role in understanding granular material behavior. This distribution is effectively quantified using a novel grading index (I_{G}), first proposed by Guida et al. (2018). The index provides a detailed characterization of the PSD shape for the specimens

$$I_{\mathrm{G}} = e^{\sqrt{\sum_i \frac{w_i}{w_{\mathrm{tot}}}(\ln s_i - \ln \bar{s})^2}} \tag{19}$$

The grading index (I_{G}) is computed based on the mass (w_i) retained on each sieve opening (d_i), the total mass of the specimen (w_{tot}), and the relative particle size (s_i), which is nondimensionalized with respect to the maximum particle size in the specimen. The relative size is expressed as $s_i = d_i / d^{\mathrm{p}}_{\mathrm{max}}$. The geometric mean of the weight distribution ($\bar{s}$) is determined by

$$\bar{s} = e^{\sum_i \frac{w_i}{w_{\mathrm{tot}}} \ln s_i} \tag{20}$$

The proposed grading index (I_{G}) provides a unique and comprehensive measure by incorporating all particle sizes, surpassing traditional metrics such as the uniformity coefficient (C_{u}) and the coefficient of curvature (C_{c}). This methodology aligns well with the strengths of DEM, which allows for the characterization of individual particles, enabling the full PSD to be captured. However, recognizing that not all particles contribute to stress transmission, an active grading index ($I_{\mathrm{G}}^{\mathrm{active}}$) is introduced. This refined index focuses exclusively on active particles involved in stress transfer, providing a more detailed representation of the active PSD ($\mathrm{PSD}^{\mathrm{active}}$).

Significant efforts have been dedicated to precisely quantifying stress transmission characteristics using a refined grading index. As a foundational step, stress transmission at the particle scale was analyzed. The effective stress tensor for the specimen was computed by aggregating the individual stress tensors of active particles, based on methodologies established in earlier studies (e.g., Weber 1966; Bagi 1996; Potyondy and Cundall 2004; Cambou et al. 2013; Love 2013). This approach integrates particle-scale stresses to determine the corresponding macroscopic stress state, that is

$$\sigma'_{ij} = \frac{1}{V} \sum_{m=1}^{N_{\mathrm{t}}} \bar{\sigma}_{ij}^{(m)} V^{(m)} \tag{21}$$

The overall effective stress tensor of the specimen σ'_{ij} is determined by aggregating the stress contributions from all particles involved in stress transmission. This tensor is computed by summing the average stress tensor $\bar{\sigma}_{ij}^{(m)}$ of each particle m, weighted by its volume $V^{(m)}$, across the total number of stress-transmitting particles N_{t}. The effective stress tensor is expressed as

$$\alpha_{ij}^{(m)} = \frac{\bar{\sigma}_{ij}^{(m)} V^{(m)}}{V}, \quad \text{for } m = 1, \ldots, N_{\mathrm{t}} \tag{22}$$

The calculation of stress transmission for individual particles, based on the previously described equations, is a straightforward process. This allows for the cumulative distribution of stress transmission to be readily determined. The refined stress-based grading index ($I_{\mathrm{G}}^{\mathrm{stress}}$) can then be computed by modifying Eq. (21), substituting w_i and w_{tot} with appropriate terms related to stress contributions

$$\frac{1-n}{\sum_{m=1}^{N_{\mathrm{t}}} V^{(m)}} p^{(m)} V^{(m)} \quad \text{and} \quad \frac{1-n}{\sum_{m=1}^{N_{\mathrm{t}}} V^{(m)}} \sum_{m=1}^{N_{\mathrm{t}}} p^{(m)} V^{(m)} \tag{23}$$

This study examines the responses of $I_{\mathrm{G}}^{\mathrm{active}}$ and $I_{\mathrm{G}}^{\mathrm{stress}}$ across varying densities and soil states under the more realistic particle property representation. The findings indicate that particle-scale stress transmission exhibits negligible variability across different packing densities and soil states. Specifically, at both peak and critical soil states, $I_{\mathrm{G}}^{\mathrm{active}}$ and $I_{\mathrm{G}}^{\mathrm{stress}}$ remain approximately 1.19, with consistently low COVs of around 0.001 across all three packing densities. These results suggest that, despite the coupled uncertainties between μ_{s} and G_{p}, their propagation has negligible impact on particle-scale stress transmission. This finding highlights that stress transmission at the particle scale is more closely linked to the PSD of the specimens, particularly for the uniform PSD used in this study. As noted by Liu et al. (2023), the effects of PSD on stress transmission are significant. While this study indicates that the coupling relationship between μ_{s} and G_{p} has limited influence on stress transmission within uniform PSD assemblies, different outcomes may arise in well-graded or gap-graded specimens. Given that PSD effects can have a more dominant impact on soil behavior, the influence of particle-scale discreteness and coupling on macroscale soil behavior generally depends on the observed soil state (e.g., peak or critical) and the specific macroscale response examined (e.g., stress ratio, stress transmission). The magnitude of this influence varies from negligible to significant across different scenarios. This analysis provides a micromechanical perspective on how realistic particle-scale characteristics shape macroscale soil

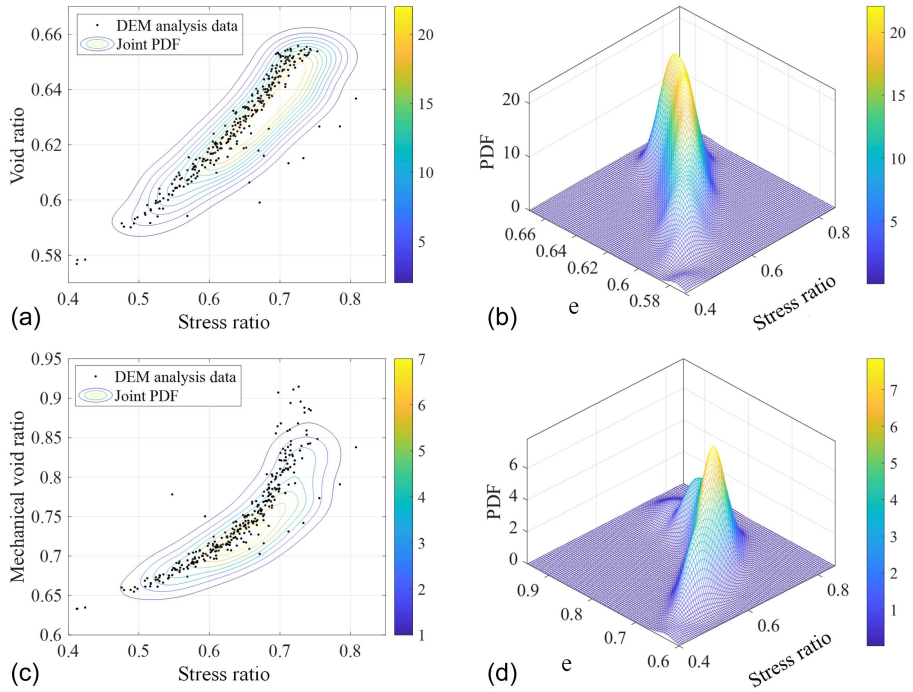

Fig. 14. Joint PDF between stress ratio and void ratio: (a) PDF contour; and (b) 3D profiles. Joint PDF between stress ratio and mechanical void ratio: (c) PDF contour; and (d) 3D profiles.

responses, offering valuable insights for improving material modeling and informing geotechnical design practices.

The decoupled M-PDEM was utilized to investigate potential dependencies among the propagated macroscale behaviors. Fig. 14 illustrates the joint PDF distributions for stress ratios, void ratio (e), and mechanical void ratio (e_m). Specifically, Figs. 14(a and b) present the joint PDFs between stress ratios and void ratios at the critical state, revealing a notable dependency between these parameters. Additionally, Figs. 14(c and d) present the joint PDFs between stress ratios and mechanical void ratios. In both cases, a nonlinear probabilistic relationship is observed, indicating that the critical void ratio tends to increase with higher critical stress ratios.

From an engineering perspective, the correlation between stress ratio and void ratio reflects the underlying micromechanical

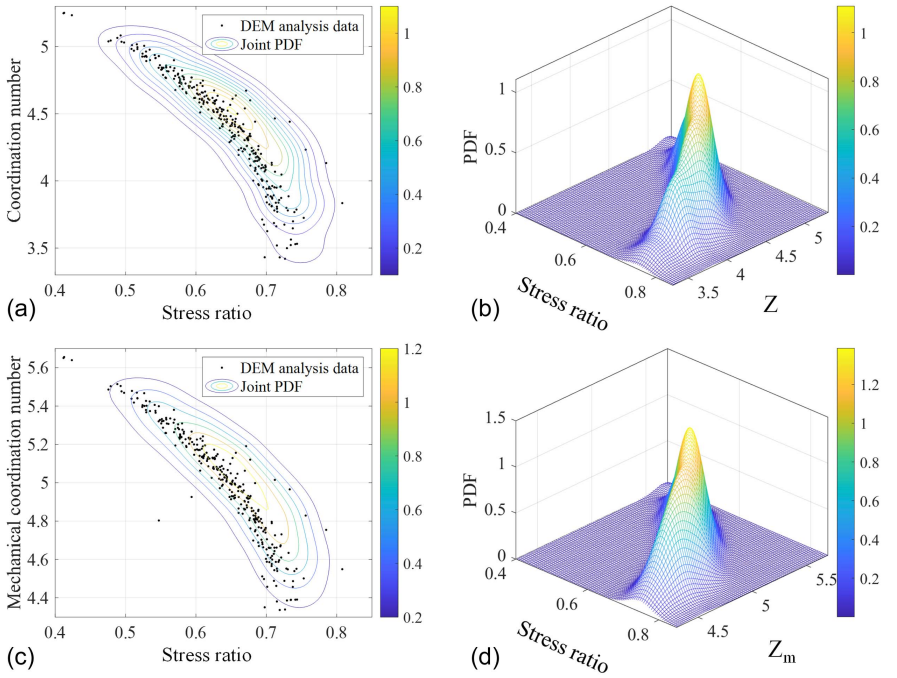

Fig. 15. (a and b) Joint PDF between stress ratio and coordination number; and (c and d) joint PDF between stress ratio and mechanical coordination number; (a) and (c) show PDF contours; and (b) and (d) show 3D profiles.

processes of granular materials, such as particle rearrangement and dilatancy. Accurately capturing this relationship is essential for predicting strength and deformation behavior in geotechnical applications. Neglecting this coupling may lead to misjudgment of critical states, thereby compromising design reliability and safety. Moreover, acknowledging that coupled particle-scale uncertainties (e.g., G_p and μ_s) collectively influence macroscale responses highlights the necessity of incorporating correlated parameters in advanced reliability analyses. Integrating these insights into practical engineering frameworks can enhance the prediction of failure modes, support the development of more resilient soil–structure interaction designs, and ultimately improve the safety and performance of geotechnical systems.

Fig. 15 illustrates the joint PDFs for stress ratio and coordination number (Z) as well as for stress ratio and mechanical coordination number (Z_m). Specifically, Figs. 15(a and b) present the PDF contours and 3D profiles for the stress ratio and Z, while Figs. 15(c and d) present the corresponding results for the stress ratio and Z_m. These findings reveal that the uncertainty propagated from the particle scale does not solely influence these key macroscale soil behaviors. Instead, they highlight a strong interdependence between these macroscale parameters, underscoring the coupled nature of their responses.

Concluding Remarks

This study proposes a framework to investigate how realistic particle-scale properties and their inherent coupling affect macroscale soil behavior. By incorporating experimentally informed variability and interdependencies of μ_s and G_p, the approach improves the physical fidelity of DEM simulations. This enables a more accurate representation of granular material heterogeneity and its impact on macroscopic responses, providing insights for geotechnical analysis and design.

- This study utilized copula theory to quantify the probabilistic dependencies among particle properties, including μ_s and G_p. This methodology enables comprehensive probability quantification of particle-scale property uncertainties, offering a more realistic representation of natural granular materials by effectively capturing the inherent variability and uncertainty across different particle properties.
- The study examined how physically representative modeling of particle-scale properties including the inherent coupling between μ_s and G_p affects macroscale soil behavior, including the stress ratio, void ratio, coordination number, and small-strain stiffness. These behaviors were analyzed through the PDF profiles of the respective parameters, presenting that the influence of uncertainties varies depending on packing densities and soil states. While uncertainties in peak stress ratios exhibited significant variability across different packing densities, they converged at the critical state, aligning with the classical soil mechanics principle of inherent consistency at critical states.
- Previous studies have demonstrated that the individual uncertainties of μ_s and G_p have minimal influence on particle-scale stress transmission, with μ_s primarily affecting large-strain behavior and G_p influencing small-strain behavior. Even when their coupled uncertainty is considered, the impact on stress transfer remains negligible. These findings suggest that particle-scale stress transmission is predominantly governed by PSD and packing structure, rather than uncertainties in particle properties. While the current studies restrict uniform PSD assemblies, different outcomes may arise for complex PSDs, including well-graded or gap-graded specimens. Given that PSD effects can have a more dominant impact on soil behavior, the influence of particle-scale discreteness and coupling on macroscale responses should be interpreted in conjunction with PSD characteristics.
- The decoupled M-PDEM analysis underscores the interlinked nature of key macroscale soil behaviors, including the stress ratio, void ratio and coordination number. Joint PDF results highlight distinct nonlinear relationships. For instance, higher critical stress ratios correlate with larger void ratios but reduced coordination numbers. These findings demonstrate that ignoring the coupled uncertainties among these parameters can lead to significant miscalculations of soil strength and deformation. By explicitly capturing these interdependencies, the proposed approach enhances the accuracy of geotechnical assessments and supports more reliable soil–structure interaction designs.

Compared to conventional deterministic analysis, this study offers a realistic representation of granular material behavior. The proposed method is broadly applicable and can accommodate a wider range of coupled uncertainties in particle properties, such as Poisson's ratio, particle shape, and other microstructural characteristics. However, this research focuses on the coupling of μ_s and G_p due to the significant challenges in experimentally obtaining high-precision data for individual particle properties. Despite current data limitations, this study establishes a framework to account for the inherent discreteness and coupled variability of particle-scale properties, highlighting the importance of physically representative modeling for reliable geotechnical analysis.

Data Availability Statement

The datasets generated and/or analyzed during this study are available from the corresponding author upon reasonable request.

Acknowledgments

The study was financially supported by the National Natural Science Foundation of China (Grant Nos. 52439001 and 12302037), the Science Fund Program for Distinguished Young Scholars (Overseas), the Research Grants Council of Hong Kong (Grant Nos. GRF 16203123, 16208224, 16217225, CRF C7085-24G, RIF R6008-24, TRS T22-607/24N, and T22-606/23-R), and the Research Funding of Tongji University (Grant No. 02002150362). The reviews and suggestions from Prof. Jianbing Chen (Tongji University) and Prof. Matthew R. Coop (University College London) are highly appreciated. The authors also acknowledge the support of HKUST in using its high-performance computing facility HPC3.

Author Contributions

Deyun Liu: Data curation; Formal analysis; Investigation; Methodology; Resources; Software; Validation; Visualization; Writing – original draft. Meng-Ze Lyu: Conceptualization; Formal analysis; Funding acquisition; Investigation; Methodology; Resources; Software; Writing – review and editing. Jidong Zhao: Conceptualization; Funding acquisition; Investigation; Methodology; Project administration; Software; Supervision; Writing – review and editing.

References

Afshari, S. S., and S. H. Pourtakdoust. 2018. "Probability density evolution for time-varying reliability assessment of wing structures." *Aviation* 22 (2): 45–54. https://doi.org/10.3846/aviation.2018.6010.

Ang, A. H. S. 2006. *Probability concepts in engineering planning and design*. 2nd ed. Hoboken, NJ: Wiley.

Ang, A. H.-S., D. De Leon, and W. Fan. 2021. "Optimal reliability-based design of complex structural systems." *Struct. Saf.* 90 (May): 102048. https://doi.org/10.1016/j.strusafe.2020.102048.

Baecher, G. B., and J. T. Christian. 2005. *Reliability and statistics in geotechnical engineering*. Hoboken, NJ: Wiley.

Bagi, K. 1996. "Stress and strain in granular assemblies." *Mech. Mater.* 22 (3): 165–177. https://doi.org/10.1016/0167-6636(95)00044-5.

Barreto, D. 2008. "Numerical and experimental investigation into the behaviour of granular materials under generalised stress states." Ph.D. thesis, Faculty of Engineering, Imperial College London.

Basarir, H., M. Kumral, C. Karpuz, and L. Tutluoglu. 2010. "Geostatistical modeling of spatial variability of SPT data for a borax stockpile site." *Eng. Geol.* 114 (3–4): 154–163. https://doi.org/10.1016/j.enggeo.2010.04.012.

Baveye, P., P. Vandevivere, B. L. Hoyle, P. C. DeLeo, and D. S. de Lozada. 1998. "Environmental impact and mechanisms of the biological clogging of saturated soils and aquifer materials." *Crit. Rev. Environ. Sci. Technol.* 28 (2): 123–191. https://doi.org/10.1080/10643389891254197.

Bazant, Z. P., and J. Planas. 2019. *Fracture and size effect in concrete and other quasibrittle materials*. Abingdon, UK: Routledge.

Cambou, B., M. Jean, and F. Radjaï. 2013. *Micromechanics of granular materials*. Hoboken, NJ: Wiley.

Cardoso, R., R. V. Silva, J. de Brito, and R. Dhir. 2016. "Use of recycled aggregates from construction and demolition waste in geotechnical applications: A literature review." *Waste Manage.* 49 (Mar): 131–145. https://doi.org/10.1016/j.wasman.2015.12.021.

Chen, H., S. Zhao, J. Zhao, and X. Zhou. 2023. "DEM-enriched contact approach for material point method." *Comput. Methods Appl. Mech. Eng.* 404 (Feb): 115814. https://doi.org/10.1016/j.cma.2022.115814.

Chen, J., J. Yang, and H. Jensen. 2020. "Structural optimization considering dynamic reliability constraints via probability density evolution method and change of probability measure." *Struct. Multidiscip. Optim.* 62 (5): 2499–2516. https://doi.org/10.1007/s00158-020-02621-4.

Chen, J., and S. Zhang. 2013. "Improving point selection in cubature by a new discrepancy." *SIAM J. Sci. Comput.* 35 (5): A2121–A2149. https://doi.org/10.1137/12089377X.

Chen, J. B., and M. Z. Lyu. 2022. "Globally-evolving-based generalized density evolution equation for nonlinear systems involving randomness from both system parameters and excitations." *Proc. R. Soc. A* 478 (2264): 20220356.

Chen, J. B., J. Y. Yang, and J. Li. 2016. "A GF-discrepancy for point selection in stochastic seismic response analysis of structures with uncertain parameters." *Struct. Saf.* 59: 20–31.

Chen, J.-B., X. Huang, and J. Li. 2024. "Quantitative property of MF-discrepancy and efficient point-selection strategy for the nonlinear stochastic response analysis of structures with random parameters." *Probab. Eng. Mech.* 78 (Oct): 103708. https://doi.org/10.1016/j.probengmech.2024.103708.

Cundall, P. A. 1988. "Computer simulations of dense sphere assemblies." In Vol. 20 of *Studies in applied mechanics*, 113–123. Amsterdam, Netherlands: Elsevier.

Cundall, P. A., and O. D. L. Strack. 1979. "A discrete numerical model for granular assemblies." *Géotechnique* 29 (1): 47–65. https://doi.org/10.1680/geot.1979.29.1.47.

Da Cruz, F., S. Emam, M. Prochnow, J.-N. Roux, and F. Chevoir. 2005. "Rheophysics of dense granular materials: Discrete simulation of plane shear flows." *Phys. Rev. E* 72 (2): 21309. https://doi.org/10.1103/PhysRevE.72.021309.

Daniel, I. M. 1994. *Engineering mechanics of composite materials*. Oxford, UK: Oxford University Press.

DeBroy, T., H. L. Wei, J. S. Zuback, T. Mukherjee, J. W. Elmer, J. O. Milewski, A. M. Beese, A. D. Wilson-Heid, A. De, and W. Zhang. 2018. "Additive manufacturing of metallic components–process, structure and properties." *Prog. Mater Sci.* 92 (Mar): 112–224. https://doi.org/10.1016/j.pmatsci.2017.10.001.

Dyson, A. P., and A. Tolooiyan. 2019. "Prediction and classification for finite element slope stability analysis by random field comparison." *Comput. Geotech.* 109 (May): 117–129. https://doi.org/10.1016/j.compgeo.2019.01.026.

Elishakoff, I. 2003. "Notes on philosophy of the Monte Carlo method." *Int. Appl. Mech.* 39 (7): 753–762. https://doi.org/10.1023/A:1026236621486.

Genest, C., B. Rémillard, and D. Beaudoin. 2009. "Goodness-of-fit tests for copulas: A review and a power study." *Insur. Math. Econ.* 44 (2): 199–213.

Griffiths, D. V., and G. A. Fenton. 2001. "Bearing capacity of spatially random soil: The undrained clay Prandtl problem revisited." *Geotechnique* 51 (4): 351–359. https://doi.org/10.1680/geot.2001.51.4.351.

Griffiths, D. V., and G. A. Fenton. 2004. "Probabilistic slope stability analysis by finite elements." *J. Geotech. Geoenviron. Eng.* 130 (5): 507–518. https://doi.org/10.1061/(ASCE)1090-0241(2004)130:5(507).

Griffiths, D. V., J. Huang, and G. A. Fenton. 2009. "Influence of spatial variability on slope reliability using 2-D random fields." *J. Geotech. Geoenviron. Eng.* 135 (10): 1367–1378. https://doi.org/10.1061/(ASCE)GT.1943-5606.0000099.

Guida, G., I. Einav, B. Marks, and F. Casini. 2018. "Linking micro grain-size polydispersity to macro porosity." *Int. J. Solids Struct.* 187 (Mar): 75–84.

Guo, N., and J. Zhao. 2014. "A coupled FEM/DEM approach for hierarchical multiscale modelling of granular media." *Int. J. Numer. Methods Eng.* 99 (11): 789–818. https://doi.org/10.1002/nme.4702.

Hai, L., and M.-Z. Lyu. 2023. "Modeling tensile failure of concrete considering multivariate correlated random fields of material parameters." *Probab. Eng. Mech.* 74 (Oct): 103529. https://doi.org/10.1016/j.probengmech.2023.103529.

He, H., C. S. Sandeep, and K. Senetakis. 2019. "The interface behavior of recycled concrete aggregate: A micromechanical grain-scale experimental study." *Constr. Build. Mater.* 210 (Jun): 627–638. https://doi.org/10.1016/j.conbuildmat.2019.03.106.

Hertz, H. 1882. "Über die Berührung fester elastischer Körper." [In German.] *J. Für Die Reine Angewandte Mathematik* 92 (156–171): 22.

Huang, X. 2014. *Exploring critical-state behaviour using DEM*. London: Imperial College.

Huang, X., K. J. Hanley, C. O'Sullivan, and C. Y. Kwok. 2014. "Exploring the influence of interparticle friction on critical state behaviour using DEM." *Int. J. Numer. Anal. Methods Geomech.* 38 (12): 1276–1297. https://doi.org/10.1002/nag.2259.

James, F. 1980. "Monte Carlo theory and practice." *Rep. Prog. Phys.* 43 (9): 1145. https://doi.org/10.1088/0034-4885/43/9/002.

Jiang, S.-H., D.-Q. Li, L.-M. Zhang, and C.-B. Zhou. 2014. "Slope reliability analysis considering spatially variable shear strength parameters using a non-intrusive stochastic finite element method." *Eng. Geol.* 168 (Jan): 120–128. https://doi.org/10.1016/j.enggeo.2013.11.006.

Kuhn, M. R., and A. Daouadji. 2018. "Quasi-static incremental behavior of granular materials: Elastic–plastic coupling and micro-scale dissipation." *J. Mech. Phys. Solids* 114 (May): 219–237. https://doi.org/10.1016/j.jmps.2018.02.019.

Kuwano, R., and R. J. Jardine. 2002. "On the applicability of cross-anisotropic elasticity to granular materials at very small strains." *Géotechnique* 52 (10): 727–749. https://doi.org/10.1680/geot.2002.52.10.727.

Li, J., and J. Chen. 2008. "The principle of preservation of probability and the generalized density evolution equation." *Struct. Saf.* 30 (1): 65–77. https://doi.org/10.1016/j.strusafe.2006.08.001.

Li, J., and J. Chen. 2009. *Stochastic dynamics of structures*. Hoboken, NJ: Wiley.

Li, J., J. Chen, W. Sun, and Y. Peng. 2012. "Advances of the probability density evolution method for nonlinear stochastic systems." *Probab. Eng. Mech.* 28 (Apr): 132–142. https://doi.org/10.1016/j.probengmech.2011.08.019.

Li, J., and D. Wang. 2023. "Comparison of PDEM and MCS: Accuracy and efficiency." *Probab. Eng. Mech.* 71 (Jan): 103382. https://doi.org/10.1016/j.probengmech.2022.103382.

Liu, D., and S. D. N. Lourenço. 2021. "Stress-dilatancy behaviour of a polymer-coated sand." *Acta Geotech.* 16 (2): 647–652. https://doi.org/10.1007/s11440-020-01022-7.

Liu, D., T. Morimoto, J. A. H. Carraro, and C. O'Sullivan. 2022. "A semi-empirical re-evaluation of the influence of state on elastic stiffness in

granular materials." *Granular Matter.* 24 (2): 56. https://doi.org/10.1007/s10035-022-01215-9.
Liu, D., C. O'Sullivan, and J. A. H. Carraro. 2021. "Influence of particle size distribution on the proportion of stress-transmitting particles and implications for measures of soil state." *J. Geotech. Geoenviron. Eng.* 147 (3): 4020182. https://doi.org/10.1061/(ASCE)GT.1943-5606.0002466.
Liu, D., C. O'Sullivan, and J. A. H. Carraro. 2023. "The influence of particle size distribution on the stress distribution in granular materials." *Géotechnique* 73 (3): 250–264. https://doi.org/10.1680/jgeot.21.00127.
Liu, D., C. S. Sandeep, K. Senetakis, V. Nardelli, and S. D. N. Lourenço. 2019. "Micromechanical behaviour of a polymer-coated sand." *Powder Technol.* 347 (Apr): 76–84. https://doi.org/10.1016/j.powtec.2019.02.030.
Liu, D. Y., and M.-Z. Lyu. 2025. "Capturing the random mechanical behaviour of granular materials: A comprehensive stochastic discrete-element method study." *Géotechnique* 75 (7): 899–912. https://doi.org/10.1680/jgeot.23.00467.
Liu, D.-Y., and M.-Z. Lyu. 2023a. "Evaluating uncertainty in particle roughness of coated sand and its implication to coating abrasion." *Powder Technol.* 430 (Jan): 118966. https://doi.org/10.1016/j.powtec.2023.118966.
Liu, D.-Y., and M.-Z. Lyu. 2023b. "Uncertainty quantification for granular materials with a stochastic discrete element method." *Comput. Geotech.* 161 (Sep): 105560. https://doi.org/10.1016/j.compgeo.2023.105560.
Liu, D.-Y., C. Wang, and M.-Z. Lyu. 2024a. "Elucidating the complexity of stress interactions in polymer-coated granular materials via copula-based probabilistic dependence configurations." *Powder Technol.* 435 (Feb): 119405. https://doi.org/10.1016/j.powtec.2024.119405.
Liu, D.-Y., M.-T. Wang, and C. Wang. 2024b. "Evaluation of mechanical behaviour of gap-graded soils with particle property disparity." *Comput. Geotech.* 167 (Mar): 106099. https://doi.org/10.1016/j.compgeo.2024.106099.
Love, A. E. H. 2013. *A treatise on the mathematical theory of elasticity.* Cambridge: Cambridge University Press.
Low, Y. M. 2013. "A new distribution for fitting four moments and its applications to reliability analysis." *Struct. Saf.* 42 (May): 12–25. https://doi.org/10.1016/j.strusafe.2013.01.007.
Lumb, P. 1966. "The variability of natural soils." *Can. Geotech. J.* 3 (2): 74–97. https://doi.org/10.1139/t66-009.
Luo, Y., and X. Q. Ai. 2022. "Wind risk assessment of urban street trees based on wind-induced fragility." *Dis. Prev. Res.* 1 (2): 7.
Lyu, M., D. Feng, X. Cao, and M. Beer. 2024a. "A full-probabilistic cloud analysis for structural seismic fragility via decoupled M-PDEM." *Earthquake Eng. Struct. Dyn.* 53 (5): 1863–1881. https://doi.org/10.1002/eqe.4093.
Lyu, M.-Z., and J.-B. Chen. 2022. "A unified formalism of the GE-GDEE for generic continuous responses and first-passage reliability analysis of multi-dimensional nonlinear systems subjected to non-white-noise excitations." *Struct. Saf.* 98 (Sep): 102233. https://doi.org/10.1016/j.strusafe.2022.102233.
Lyu, M.-Z., J.-B. Chen, and J.-X. Shen. 2024b. "Refined probabilistic response and seismic reliability evaluation of high-rise reinforced concrete structures via physically driven dimension-reduced probability density evolution equation." *Acta Mech.* 235 (3): 1535–1561. https://doi.org/10.1007/s00707-023-03666-4.
Lyu, M.-Z., Z.-J. Fei, and D.-C. Feng. 2024c. "Vine-copula-based multi-dimensional fragility analysis of nuclear power plant under sequential earthquakes." *Struct. Saf.* 110 (Sep): 102494. https://doi.org/10.1016/j.strusafe.2024.102494.
Lyu, M.-Z., Z.-J. Fei, and D.-C. Feng. 2024d. "Copula-based cloud analysis for seismic fragility and its application to nuclear power plant structures." *Eng. Struct.* 305 (Apr): 117754. https://doi.org/10.1016/j.engstruct.2024.117754.
Lyu, M.-Z., D.-C. Feng, J.-B. Chen, and J. Li. 2024e. "A decoupled approach for determination of the joint probability density function of a high-dimensional nonlinear stochastic dynamical system via the probability density evolution method." *Comput. Methods Appl. Mech. Eng.* 418 (Jan): 116443. https://doi.org/10.1016/j.cma.2023.116443.
Mahadevan, S., and A. Haldar. 1991. "Practical random field discretization in stochastic finite element analysis." *Struct. Saf.* 9 (4): 283–304. https://doi.org/10.1016/0167-4730(91)90050-J.
Majmudar, T. S., and R. P. Behringer. 2005. "Contact force measurements and stress-induced anisotropy in granular materials." *Nature* 435 (7045): 1079–1082. https://doi.org/10.1038/nature03805.
Nardelli, V., and M. R. Coop. 2019. "The experimental contact behaviour of natural sands: Normal and tangential loading." *Géotechnique* 69 (8): 672–686. https://doi.org/10.1680/jgeot.17.P.167.
Nardelli, V., M. R. Coop, J. E. Andrade, and F. Paccagnella. 2017. "An experimental investigation of the micromechanics of Eglin sand." *Powder Technol.* 312 (May): 166–174. https://doi.org/10.1016/j.powtec.2017.02.009.
Nelsen, R. B. 2006. *An introduction to Copulas*. 2nd ed. New York: Springer.
Nielsen, S. R. K., Y. B. Peng, and M. T. Sichani. 2016. "Response and reliability analysis of nonlinear uncertain dynamical structures by the probability density evolution method." *Int. J. Dyn. Control* 4 (2): 221–232. https://doi.org/10.1007/s40435-015-0155-4.
O'Sullivan, C. 2011. *Particulate discrete element modelling: A geomechanics perspective*. Boca Raton, FL: CRC Press.
Phoon, K.-K., and F. H. Kulhawy. 1999. "Characterization of geotechnical variability." *Can. Geotech. J.* 36 (4): 612–624. https://doi.org/10.1139/t99-038.
Phoon, K.-K., and F. H. Kulhawy. 2008. "Serviceability limit state reliability-based design." In *Reliability-based design in geotechnical engineering*, 356–396. Boca Raton, FL: CRC Press.
Potts, D. M., L. Zdravković, T. I. Addenbrooke, K. G. Higgins, and N. Kovačević. 2001. Vol. 2 of *Finite element analysis in geotechnical engineering: Application*. London: Thomas Telford.
Potyondy, D. O., and P. A. Cundall. 2004. "A bonded-particle model for rock." *Int. J. Rock Mech. Min. Sci.* 41 (8): 1329–1364. https://doi.org/10.1016/j.ijrmms.2004.09.011.
Rahimi, S., C. M. Wood, and L. M. Wotherspoon. 2020. "Influence of soil aging on SPT-Vs correlation and seismic site classification." *Eng. Geol.* 272 (Jul): 105653. https://doi.org/10.1016/j.enggeo.2020.105653.
Sandeep, C. S., H. He, and K. Senetakis. 2018. "An experimental micromechanical study of sand grain contacts behavior from different geological environments." *Eng. Geol.* 246 (Nov): 176–186. https://doi.org/10.1016/j.enggeo.2018.09.030.
Sandeep, C. S., and K. Senetakis. 2018. "Effect of Young's modulus and surface roughness on the inter-particle friction of granular materials." *Materials* 11 (2): 217. https://doi.org/10.3390/ma11020217.
Senetakis, K., and M. Coop. 2014. "The development of a new micromechanical inter-particle loading apparatus." *Geotech. Test. J.* 37 (6): 1028–1039. https://doi.org/10.1520/GTJ20120187.
Senetakis, K., and C. S. Sandeep. 2017. "Experimental study of sand grains behavior at their contacts with force-and displacement-controlled sliding tests." *Underground Space* 2 (1): 38–44. https://doi.org/10.1016/j.undsp.2017.03.001.
Shire, T., C. O'Sullivan, K. J. Hanley, and R. J. Fannin. 2014. "Fabric and effective stress distribution in internally unstable soils." *J. Geotech. Geoenviron. Eng.* 140 (12): 04014072. https://doi.org/10.1061/(ASCE)GT.1943-5606.0001184.
Snoeijer, J. H., T. J. H. Vlugt, M. van Hecke, and W. van Saarloos. 2004. "Force network ensemble: A new approach to static granular matter." *Phys. Rev. Lett.* 92 (5): 54302. https://doi.org/10.1103/PhysRevLett.92.054302.
Song, Y., B. Basu, Z. Zhang, J. D. Sørensen, J. Li, and J. Chen. 2021. "Dynamic reliability analysis of a floating offshore wind turbine under wind-wave joint excitations via probability density evolution method." *Renew. Energy* 168 (May): 991–1014. https://doi.org/10.1016/j.renene.2020.12.093.
Sufian, A., M. Artigaut, T. Shire, and C. O'Sullivan. 2021. "Influence of fabric on stress distribution in gap-graded soil." *J. Geotech. Geoenviron. Eng.* 147 (5): 04021016. https://doi.org/10.1061/(ASCE)GT.1943-5606.0002487.
Tao, J., J. Chen, and X. Ren. 2020. "Copula-based quantification of probabilistic dependence configurations of material parameters in damage

constitutive modeling of concrete." *J. Struct. Eng.* 146 (9): 4020194. https://doi.org/10.1061/(ASCE)ST.1943-541X.0002729.
Thompson, A. P., et al. 2022. "LAMMPS-a flexible simulation tool for particle-based materials modeling at the atomic, meso, and continuum scales." *Comput. Phys. Commun.* 271 (Feb): 108171. https://doi.org/10.1016/j.cpc.2021.108171.
Thornton, C. 2000. "Numerical simulations of deviatoric shear deformation of granular media." *Géotechnique* 50 (1): 43–53. https://doi.org/10.1680/geot.2000.50.1.43.
Tian, Y., and K. Senetakis. 2022. "On the contact problem of soft-rigid interfaces: Incorporation of Mindlin-Deresiewicz and self-deformation concepts." *Granular Matter.* 24 (1): 28. https://doi.org/10.1007/s10035-021-01186-3.
Vanmarcke, E. H. 1977. "Probabilistic modeling of soil profiles." *J. Geotech. Eng. Div.* 103 (11): 1227–1246. https://doi.org/10.1061/AJGEB6.0000517.
Wang, D., and J. Li. 2020. "A reproducing kernel particle method for solving generalized probability density evolution equation in stochastic dynamic analysis." *Comput. Mech.* 65 (3): 597–607. https://doi.org/10.1007/s00466-019-01785-1.
Weber, J. 1966. "Recherches concernant les contraintes intergranulaires dans les milieux pulvérulents." *Bulletin de Liaison Des Ponts-et-Chaussées* 20 (Jul): 1–20.
Wu, M., J. Wang, and B. Zhao. 2022. "DEM modeling of one-dimensional compression of sands incorporating statistical particle fragmentation scheme." *Can. Geotech. J.* 59 (1): 144–157. https://doi.org/10.1139/cgj-2020-0308.
Xu, J., and F. Kong. 2018. "A new unequal-weighted sampling method for efficient reliability analysis." *Reliab. Eng. Syst. Saf.* 172 (Apr): 94–102. https://doi.org/10.1016/j.ress.2017.12.007.
Xu, L., and W. Zhai. 2017. "A novel model for determining the amplitude-wavelength limits of track irregularities accompanied by a reliability assessment in railway vehicle-track dynamics." *Mech. Syst. Sig. Process.* 86 (Mar): 260–277. https://doi.org/10.1016/j.ymssp.2016.10.010.
Yan, Z., S. K. Wilkinson, E. H. Stitt, and M. Marigo. 2015. "Discrete element modelling (DEM) input parameters: Understanding their impact on model predictions using statistical analysis." *Comput. Particle Mech.* 2 (3): 283–299. https://doi.org/10.1007/s40571-015-0056-5.
Zhang, L.-W., Z.-H. Lu, and Y.-G. Zhao. 2021. "Dynamic reliability assessment of nonlinear structures using extreme value distribution based on L-moments." *Mech. Syst. Sig. Process.* 159 (Oct): 107832. https://doi.org/10.1016/j.ymssp.2021.107832.
Zhao, J., S. Zhao, and S. Luding. 2023. "The role of particle shape in computational modelling of granular matter." *Nat. Rev. Phys.* 5 (9): 505–525.
Zhao, S., T. M. Evans, and X. Zhou. 2018. "Effects of curvature-related DEM contact model on the macro- and micro-mechanical behaviours of granular soils." *Géotechnique* 68 (12): 1085–1098. https://doi.org/10.1680/jgeot.17.P.158.
Zhao, Y.-G., and Z.-H. Lu. 2007. "Fourth-moment standardization for structural reliability assessment." *J. Struct. Eng.* 133 (7): 916–924. https://doi.org/10.1061/(ASCE)0733-9445(2007)133:7(916).
Zhou, H., J. Li, and X. Ren. 2016. "Multiscale stochastic structural analysis toward reliability assessment for large complex reinforced concrete structures." *Int. J. Multiscale Comput. Eng.* 14 (3): 303–321.